Universiteit Utrecht

Effect of Hydrothermal Treatment and Chemical Deactivation on the Activity of Cu-SSZ-13 in NH_3-SCR

Master's Research Project

Pasi Paalanen
Student number: 3755894

September 3, 2013

Supervisors:
Dr. Inés Lezcano-Gonzalez
Dr. Pieter Bruijnincx
Prof. Dr. Ir. Bert Weckhuysen

Inorganic Chemistry and Catalysis
University of Utrecht

Abstract

The effect of hydrothermal treatment and chemical deactivation on the Ammonia Selective Catalytic Reduction (NH_3-SCR) with Cu-SSZ-13 zeolite as the catalyst has been studied. The Cu-SSZ-13 samples were first hydrothermally treated at 730 °C for 13h and then subsequently individually impregnated via Wet Impregnation method with the chosen chemical species, with either Ca, P, Pt or Zn. The samples were characterized with XRD, IR, UV-Vis and/or N_2 physisorption methods and catalytic tests were performed under the Standard SCR reaction conditions within a temperature range of 150-450 °C. Hydrothermal treatment caused considerable catalyst deactivation due to clustering of the catalytically active Cu^{2+} ion to inactive Cu oxides. Impregnation with Pt caused formation of Pt^0 on the hydrothermally treated Cu-SSZ-13 catalyst which resulted in severe loss in the reaction selectivity. P-impregnation caused complete deactivation of the Cu-SSZ-13 up to reaction temperature of 350 °C due to unidentified P-species. Ca and Zn impregnations resulted in less severe catalyst deactivation than the P and Pt impregnations. For Ca, presence of Ca^{2+} was observed but the deactivating species was not definitely identified while for the Zn-impregnation catalyst deactivation was caused by the formed ZnO.

Table of Contents

1 INTRODUCTION

Selective Catalytic Reduction with ammonia (NH_3-SCR) is being used, as well as in other combustion power sources, in diesel engines for the abatement of environmentally harmful NO_x (x=1,2) gases present in the exhaust fume. In the NH_3-SCR process, NH_3 is used as a reductive agent to reduce NO_x to N_2 and H_2O, both of which are environmentally harmless gases and naturally present in the atmosphere.[1] Of NO_x from road traffic, 75% is emitted by diesel engines. On coming years, more stringent emission regulations are being applied by European Union to limit NO_x released to the atmosphere.[1] Therefore, on-going research efforts aim to improve the catalysts used for NH_3-SCR to gain more efficient and suitable NH_3-SCR systems to be used with diesel engines in the exhaust fume treatment.

Several metal-containing zeolites have been studied in the past but were shown to have unsatisfactory performance for use in the NH_3-SCR with diesel vehicles either due to insufficient conversion activity, selectivity and/or stability under operating conditions.[1–7] Either the metals show low activity for conversion, e.g. Co, Ni and Zn, or highly oxidizing metals, such as Pt, Pd and Rh, were unselective for the reaction causing formation of undesired ozone depleting N_2O.[1] Besides metal-containing zeolites, V oxide (V_2O_3) based catalysts have been used successfully on commercial applications on stationary systems, such as power plants, but due to the toxic properties of V these catalysts are unsuitable for mobile applications.[8]

Deactivating phenomena present in the real operating environment of NH_3-SCR in applications for diesel engines cause activity loss on metal-zeolites.[6] Hydrothermal aging i.e. reaction conditions in the presence of heat and water, degrades the zeolite framework structure causing loss of surface area of the catalyst and sintering of metal particles into catalytically inactive metal clusters.[6] Chemical deactivation is caused by chemical species, such as P, Zn, Ca, Mg, Pt, S or K, which can be present in the exhaust fume rendering the catalyst inactive.[9–11] Of these mentioned deactivating effects, hydrothermal aging and sintering have received more attention so far, while the chemical deactivation effects on catalyst activity in NH_3-SCR are less studied.

For the current knowledge, introduction of the Cu to SSZ-13 (CHA framework type) has shown the most promising properties with good activity for the NH_3-SCR reaction starting from low temperatures when compared to other metal exchanged zeolites, good selectivity for NO_x conversion to N_2 without formation of undesired side-product N_2O and with excellent hydrothermal

stability,[2,3,12,13] all of which properties are desirable for a usable catalyst under the real NH_3-SCR operation conditions.

While the hydrothermal aging of the Cu-SSZ-13 has received more research attention so far, the chemical deactivation effects on Cu-SSZ-13, to our best knowledge, are completely unstudied up-to-date and need to be resolved for continued improvement of the commercial application of Cu-SSZ-13 in NH_3-SCR NO_x abatement systems. This study aims to resolve the combined effect of hydrothermal conditions and catalyst deactivation by chemical species, on activity and selectivity of Cu-SSZ-13 in NH_3-SCR. The catalyst deactivating species Ca, P, Pt and Zn were chosen to be studied individually as their effect might be expected to be most detrimental on the catalyst activity.

To study the effect of hydrothermal conditions and chemical deactivation, first the Cu-SSZ-13 samples are treated under hydrothermal conditions and then subsequently impregnated with one of the deactivating chemical species. The hydrothermally treated samples are to be characterized by XRD and IR and for the characterization of hydrothermally treated and subsequently chemically deactivated samples, XRD, UV-Vis and N_2 physisorption are used. Both, the only hydrothermally aged and subsequently chemically deactivated Cu-SSZ-13 samples, are tested for their catalytical activity in NH_3-SCR under the Standard SCR reaction conditions.

1.1 NH_3-SCR

The modern lean combustion engines operate under oxygen excess which has rendered the older three-way catalysts obsolete for the removal of NO_x gases from the exhaust fume. As an alternative technique, NH_3-SCR has been introduced to be used conjunctly with lean combustion engines as

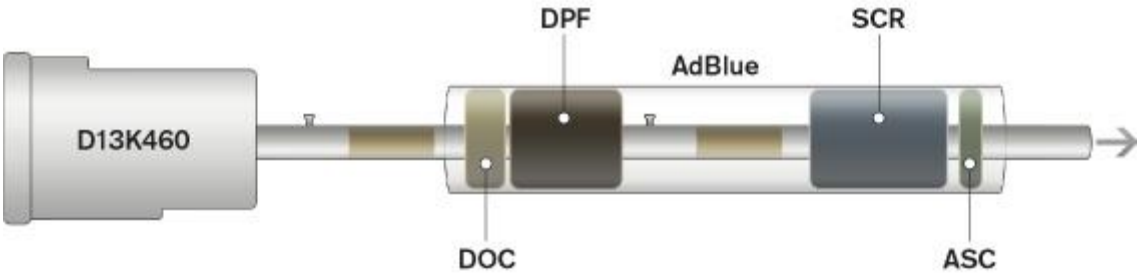

Figure 1: A schematical presentation of an exhaust gas treatment system from Volvo Trucks operating under oxygen excess conditions. The NH_3-SCR reactions described in this article take place in the SCR component depicted above. Abbreviations: Diesel Oxidative Catalyst (DOC), Diesel Particulate Filter (DPF), AdBlue (source for NH_3), Selective Catalytic Reduction (SCR), Ammonia Slip Catalyst (ASC). Picture from: http://www.volvotrucks.com/ (20.03.2013)

NH_3-SCR can operate under oxygen excess conditions.[1] As an example of modern combustion engine exhaust gas treatment system where NH_3-SCR catalyst is one of the components, a schematical drawing is presented in Figure 1 of a commercial diesel engine exhaust gas treatment system from Volvo Trucks.

In the NH_3-SCR reaction, the NO_x gases are reduced to N_2 and H_2O with the use of NH_3 fed to the exhaust stream (in Figure 1, AdBlue is the trademark name for the NH_3 source) as a reductive agent. Depending on the composition of the input gas, the NH_3-SCR reaction proceeds through three major pathways over zeolites;[14]

The Standard SCR reaction $4NH_3 + 4NO + O_2 \rightarrow 4N_2 + 6H_2O$ (1)

The Fast SCR reaction $2NH_3 + NO + NO_2 \rightarrow 2N_2 + 3H_2O$ (2)

The NO_2 SCR reaction $4NH_3 + 3NO_2 \rightarrow 3.5N_2 + 6H_2O$ (3)

In the Standard SCR reaction (1), NH_3 and NO are fed in a stoichiometric ratio of 1:1 and it is the reaction to be studied in the present project. The Fast SCR reaction (2) occurs when NO and NO_2 are present in the input feed in ratio of 1:1, and proceeds faster than the Standard SCR reaction (1).[1] When the NO_2:NO_x ratio exceeds ½, the NO_2 SCR reaction (3) takes place. Pathways in the presence of NO_2 in the feed gas are important as real combustion exhaust fume also contains NO_2 in the feed.[1] Besides the mentioned main reactions, as a side-reaction unwanted N_2O can be formed,[1] and also additionally, under the Standard SCR reaction conditions (1) NO_2 can be found in the exhaust fume,[2,6] and can therefore be considered as a by-product in the Standard SCR reaction (1).

The mechanism under which the NH_3-SCR reaction is thought to proceed over metal-exchanged zeolites is discussed in the review article by Brandenberger *et al.*[1] In general, over metal-exchanged zeolites, oxidation of NO to NO_2 at the metal sites is thought to be the rate determining step which results in adsorpted NO_2 on the catalyst surface. NH_3 is thought to adsorb and form an activated NH_3 species over the Brønsted acid sites in the framework structure. The activated NH_3 on Brønsted acid sites and the adsorpted NO_2 are then thought to react and form intermediates (NH_4NO_3, HNO_3, HNO_2, N_2O_3) on the catalyst surface. The formed intermediate depends on the several possible reaction routes over which the reaction is optionally thought to proceed. Regardless the route, formed intermediates have been further proposed to react with additional NH_3 or NO to form NH_4NO_2 as the final intermediate which is decomposed to N_2 and H_2O, i.e. irrespective the reaction route the last formed intermediate is NH_4NO_2 which decomposes to the reaction products. More complete and detailed discussion about the reaction mechanism over various possible routes in

NH_3-SCR over metal exchanged zeolites, including side-product formations, can be found in the review article by Brandenberger *et al.*[1]

However, whether the general mechanism proposed above applies when Cu-SSZ-13 is used as the catalyst is uncertain and the reaction mechanism of NH_3-SCR over Cu-SSZ-13 is yet not well-established. As some differences to the general mechanism over metal-exchanged zeolites, on Cu-SSZ-13, NH_3 has also been observed to adsorb on Cu sites as well as on the framework Brønsted acid sites,[15–17] and the NO oxidation step has been observed not to play any significant role in NH_3-SCR over Cu-SSZ-13 i.e. NO oxidation might not be the rate determining step.[13]

The NH_3 adsorption on Cu sites has been observed to take place from lower temperatures of 100-150 °C,[15–17] up to at least 350 °C.[17] Under Fast SCR conditions (2), Yang *et al.* have suggested for Cu-SSZ-13 that Cu sites where NH_3 adsorbs are the active parts for the NH_3-SCR while NH_3 adsorpted on the Brønsted acid sites are inactive. At low temperatures (150 ˚C), before the NH_3-SCR reaction takes place, it was suggested that the Brønsted acid sites were first saturated with NH_3 after which NH_3 also started to reach the active Cu sites and only then the NO_x to N_2 conversion took place. Upon raising the reaction temperature (to 300 ˚C), Yang *et al.* suggested that the Brønsted site adsorpted NH_3 might migrate to active Cu sites where it may react with NO_x to form N_2.[16] Under both, Fast (2) and Standard SCR (1) reaction conditions over Cu-SSZ-13, Zhu *et al.* observed that NH_3 adsorpted on Cu sites reacts preferentially and faster with NO_x than the Brønsted site adsorpted NH_3.[17] Regarding the NO oxidation step which was considered to be rate determining in the general NH_3-SCR mechanism over the metal-exchanged zeolites as discussed prior, Kwak *et al.* observed good NO conversions on both Fast and Standard SCR reactions over Cu-SSZ-13 without any significant NO oxidation activity, and suggested that the NO oxidation does not have significant role in the NH_3-SCR on Cu-SSZ-13.[13]

1.2 Deactivation phenomena in NH_3-SCR

The phenomena causing loss of catalyst activity and/or selectivity towards the desired reaction are either of chemical, mechanical or thermal origin.[18] Within chemical deactivation are encompassed the deactivation of the catalytically active sites by strong chemisorption of unwanted species or reactions of catalytically active species with species present in reaction environment, forming catalytically inactive species. By mechanical deactivation are meant the physical deposition of species on the catalyst surface, such as coke deposition, and also loss of catalyst surface area or active sites due to attrition or crushing of catalyst. And lastly, thermal deactivation is defined as loss of catalyst support area by degradation of the catalyst framework or by loss of active catalyst

species by the process of sintering in which catalytically active species agglomerate to form larger, inactive species due to weak interaction of the catalytically active species with the catalysts surface.[18,19]

The NH_3-SCR reaction with diesel engines takes place under hydrothermal conditions, i.e. in the presence of heat and water, and causes zeolites to undergo thermal deactivation through degradation of the framework structure by loss of Al-atoms from the framework. This process is called dealumination and is presented schematically in Figure 2, as according to Masuda *et al.*[20] In the process of dealumination, the nucleophilic water molecules react with the electrophilic zeolite framework aluminium (Al_F in the Figure 2) removing it from the zeolite framework and causing the eventual formation of extra framework aluminium species (Al_E in the Figure 2), as either condensed or non-condensed phases, leaving behind to the zeolite framework a hole, i.e. hydroxyl nest or other defect group.[21] Condensed phases are thought to incorporate polymeric non-hydroxyl containing species e.g. Al_2O_3 while non-condensed species are thought to contain hydroxy groups coordinated to aluminium, e.g. $Al(OH)_6$.[20,22,23] Besides fully being removed from the zeolite framework, Al may

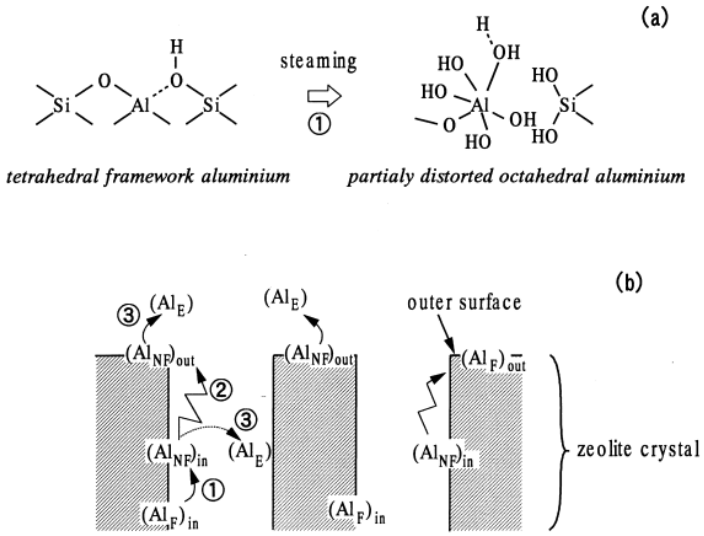

Figure 2: Description of the dealumination process in zeolites as induced by hydrothermal conditions. (a) formation of partially distorted aluminium which is still partly attached to the zeolite (b) formation of extra-framework aluminium. Abbreviations Al_F, Al_{NF} and Al_E refer to framework aluminium, partially distorted aluminium and extra-framework aluminium, respectively. Picture from reference 20.

also remain in the framework as a partially distorted Al species (Al_{NF} in the Figure 2) which still have some unbroken bonds to the zeolite framework if the dealumination does not proceed to the end.[20,22,23] As the formed hydroxyl nests or other defect groups mostly bear no charge,[21,24] the charge balancing cations no longer have any anchoring site on the framework and are subject to sintering and formation of clustered inactive species causing loss of catalytic activity.[18,19]

In the diesel engine exhaust fume, a variety of chemical species are present which may cause deactivation of the catalyst in NH_3-SCR by chemical deactivation.[9–11] Substances such as P, Ca, Mg and Zn originate to the exhaust stream from oil additives. S is usually present as an impurity in fuel and engine oil. K used in production of biodiesel can also be found from the exhaust stream as impurity and other traces of alkaline elements are due to impurities in urea solution used as the source for the NH_3 reductive agent.[11] From structural degradation of the engine structures: Fe, Cu, Al and Cr can also be found from the downstream NH_3-SCR catalyst,[11] while traces of Pt can be introduced to exhaust stream from degradation of Diesel Oxidative Catalyst (DOC) in which Pt is the active compound and is located upstream from the NH_3-SCR catalyst in the real commercial exhaust systems (Figure 1).[6] Also, incompletely burned hydrocarbons may be present in the exhaust fume, depositing on the catalyst,[4,9] but are not a major concern for the NH_3-SCR as incompletely burned hydrocarbons are mostly oxidized by the upstream DOC before reaching the NH_3-SCR component (Figure 1).

In general, under real diesel engine operating conditions with variety of different types of catalysts, the deactivation due to chemical species is most commonly caused by formation of overlaying chemical species over the catalyst surface.[10,25] The overlaying species cause diffusion limitations, limiting the reaction rate by reducing the reactant accessibility to the active sites and therefore effectiveness of the catalyst.[10,14,25] Comparable chemical deactivation results have also been found for metal-exchanged zeolites used to catalyze the NH_3-SCR reaction.[4,9,26] Alternatively, besides creating species causing diffusion limitations, compounds present under reaction conditions may also react with the catalytically active species of the catalyst creating inactive phases.[18,26,27] Such formed inactive species have been observed, in case of Cu-ZSM-5 where under hydrothermal reaction conditions Cu has been found to form catalytically inactive $CuAl_2O_4$ in reaction with the extra-framework Al species.[27] In a study by Kern *et al.* about deactivation of the Fe-MFI catalyst, P might have been able coordinate with active Fe sites possibly causing lost activity towards the NH_3-SCR.[26]

1.3 Cu-SSZ-13 zeolite

Aluminosilicate zeolites contain SiO_4 and AlO_4 tetrahedra as the primary building units which connect to each other via a bridging oxygen. Each tetrahedra centered on Al contains one negative charge causing overall negative charge on the zeolite framework which needs to be compensated by extra-framework cations. The three dimensional zeolite framework formed from the interconnected Si and Al tetrahedras contains framework penetrating channels, channel intersections and cages with dimensions of 0.2-1.0 nm, which host the extra-framework cations.[28] As the cations present in the zeolite channels area usually rather mobile, they may be exchanged to desired cationic species via ion-exchange methods creating catalytically active sites on the zeolite.[28]

Cu-SSZ-13 is an aluminosilicate zeolite that contains Cu^{2+}-ions as the charge compensating cations in the framework structure. Cu-SSZ-13 zeolite possesses a chabazite (CHA) framework structure (Figure 3) with channel size at the double six-membered ring (d6r) of about 0.38 nm (3.8Å).[2] As a catalyst for NH_3-SCR, Cu-SSZ-13 has been found to be very active and selective towards formation of N_2 over a wide temperature range of 150 °C – 550 °C,[2,12,29] and also showing good hydrothermal stability up to temperatures of 800 °C, which is a significant achievement as compared to other zeolites.[3–6] The hydrothermal stability is assigned to be due to the Cu^{2+} location on the d6r subunit, as diffusion pathways energies from the location are deemed to be high and therefore even at high temperatures the Cu^{2+} ion remains at the same d6r location.[30] The high

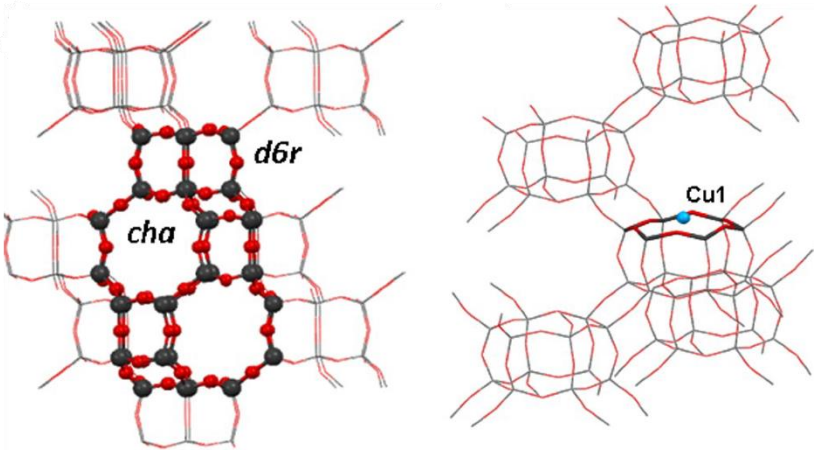

Figure 3: Crystal structure of the chabazite (CHA) zeolite framework (left). On the right side, Cu-SSZ-13 zeolite in which Cu^{2+}-ion is shown to locate on the double six-membered ring (d6r). Red color represents O atoms, black Si or Al and blue Cu^{2+}-ion. Picture from reference 31.

catalytic activity of Cu-SSZ-13 is also most likely due to location of the isolated Cu^{2+} ion on the d6r framework subunit.[15,29,31] The good selectivity of Cu-SSZ-13 towards N_2 has also been assigned to relate the isolated Cu^{2+} location,[29] as mono(μ-oxo) dicopper species which are thought to catalyze formation of undesired N_2O, have not been observed with Cu-SSZ-13.[12,32] Also, as an additional advantage of using the Cu-SSZ-13 as the catalyst for NH_3-SCR is that it has been found to resist propene poisoning better, in comparison to other zeolites used in NH_3-SCR.[4]

2 EXPERIMENTAL

2.1 The synthesis of SSZ-13 zeolite, ion-exchange and impregnation

The synthesis of SSZ-13 was performed following a sol-gel method by Diaz-Cabañaz *et al.* with the exception of Al in the framework structure.[33] To achieve a Si:Al ratio of 15, 47.55 g of tetraethyl orthosilicate (TEOS), 2.33 g of aluminium isopropoxide ($Al(O\text{-}i\text{-}Pr)_3$) and 102.43 g of 21 wt-% N,N,N-trimethyladamantammonium hydroxide (TMAdaOH) were mixed in a beaker and the formed solution was set to evaporate with constant mixing with a magnetic rod, in room temperature for four days until solution weight reached 83.24 g. Into the concentrated solution, 4.71 g 51 wt-% aqueous hydrofluoric acid (HF) was mixed and the resulting mixture was divided into three Teflon-lined autoclaves. Autoclaves were inserted into oven pre-heated to 150 °C, and left there for six days to form the desired SSZ-13 framework. Removal of the autoclaves was followed by washing the synthesis mixtures from each autoclave with approximately 3000 ml of distilled water, with the use of vacuum filtration. Washed samples were set to dry to an oven at 60 °C for overnight. Drying was followed by calcination (calcination program in Appendix, Figure B-1) the as-synthesized SSZ-13 samples to remove the TMAdaOH template from the pores of the zeolite and to form the acid form, H-SSZ-13, of the zeolite. To ensure complete template removal, samples were calcined in small 1.0-1.5 g batches. In total, 10.60 g of H-SSZ-13 was obtained from the synthesis after calcination.

The synthesized H-SSZ-13 was further ion-exchanged via the Aqueous Ion-exchange method to introduce the Cu^{2+}-ion as the charge compensating cation to the zeolite framework.[1] Different amounts of H-SSZ-13 were exchanged at the time, each of which with nominal Cu-loading of 2 wt-%. As an example of the procedure, a mixture of 165.91 ml of distilled water and 4.14 g of copper(II) sulphate pentahydrade ($CuSO_4 \cdot 5\ H_2O$) was prepared into a closable water bath glass to obtain water solution of the $CuSO_4$. A magnetic rod was added for constant mixing of the $CuSO_4$ solution and the solution was pre-heated to 80 °C using the closed water bath. After the solution reached the temperature of 80 °C, 3.32 g of H-SSZ-13 was added to the $CuSO_4$ solution and the H-SSZ-13 + $CuSO_4$ mixture was left dwelling for 2h at 80 °C. After 2h, the $CuSO_4$ + H-SSZ-13 solution was washed using vacuum filtration with approximately 3000 ml of distilled water and set to dry to an oven at 60 °C for overnight. Finally, the dried Cu-SSZ-13 samples were calcined in small batches of 1.34 g and 1.77 g using a temperature program described in Appendix Figure B-2. After calcination,

3.05 g of ready Cu-SSZ-13 catalyst was obtained. Identical process was reproduced for the H-SSZ-13 from the other two autoclaves producing amounts of 4.04 g and 2.86 g of ready Cu-SSZ-13 catalyst.

To mimic the catalyst deactivation under hydrothermal conditions in NH_3-SCR, the previously synthesized samples of Cu-SSZ-13 were first steamed at 730 °C and then subsequently Wet Impregnated with either Ca, P, Pt or Zn as the deactivating species. For all impregnations, nominal loading of 2 wt-% of the impregnating species was used. For the prepared Ca, P and Zn samples, the steamed Cu-SSZ-13 parent was the same (i.e. from the same autoclave), for Pt the steamed Cu-SSZ-13 originated from a different parent (i.e. from different autoclave). More discussion about the steaming procedure in the later section 2.3 where the steaming set-up used is introduced.

For the impregnation with P, diammonium hydrogen phosphate ($(NH_4)_2HPO_4$), was used as the P-precursor. 3.13 g of $(NH_4)_2HPO_4$ was mixed with 10 ml of MilliQ water in a measuring flask. 1.00 g of steamed Cu-SSZ-13 catalyst was added to a boiling flask with a magnetic rod. 280 µl of prepared $(NH_4)_2HPO_4$ solution was added using an auto pipette, into the boiling flask with the steamed catalyst sample. For 1h hour, the impregnated slurry was homogenized with mixing with the magnetic rod. After homogenization, sample was shortly dried at ~120 °C to get it off from the flask walls and then calcined with the temperature program presented in the Appendix Figure B-3. Same procedure as for P impregnation was used for Ca, Pt and Zn impregnations also. For Zn, 7.05 g of zinc nitrate hexahydrate ($Zn(NO_3)_2{\cdot}6H_2O$) was mixed with 10 ml of MilliQ water to impregnate 1.00 g of steamed catalyst. Ca sample was prepared with 5.60 g of calcium nitrate tetrahydrate ($Ca(NO_3)_2{\cdot}4H_2O$) mixed with 10 ml of MilliQ water to impregnate 1.00 g steamed catalyst. For Pt, the procedure was slightly different due to poor solubility of tetraammineplatinum(II) nitrate ($Pt(NH_3)_4(NO_3)_2$) used as the Pt-precursor. 47 mg of $Pt(NH_3)_4(NO_3)_2$ was mixed with 1 ml of MilliQ water and 1.00 g of catalyst was impregnated with 880 µl of prepared solution, instead of the 280 µl used for the other impregnations. Due to higher water amount used, the calcination program duration was increased as compared to other samples and the program described in Appendix Figure B-3 was used.

2.2 Characterization methods

As methods to characterize the prepared samples, methods of X-ray Diffraction (XRD), Ultraviolet-Visible spectroscopy (UV-Vis), Infrared spectroscopy (IR) and N_2 physisorption were employed.

The in-house Bruker D2 Phaser diffractometer was used for the XRD measurements to characterize the crystalline structures present in the samples. All samples were scanned with

coupled 2θ mode over a 2θ range of 5-60°. Step size of 0.016° of 2θ with collection time of 0.7 s per step, were used. Co K_α was used as the radiation source. Bruker DIFFRACplus evaluation software with PDFmaint database was used to identify the crystalline structures.

UV-Vis measurements were performed with in-house Varian Cary-500 UV-Vis-NIR (NIR, Near Infrared) instrument. Collection range for the spectra was 4000-50 000 cm^{-1} (UV-Vis-NIR range). As a background, same pre-measured data file was used for each performed measurement and the scan rate of 6000 cm-^{1}/min with data interval of 10 cm^{-1} was used.

The IR studies were performed using Perkin-Elmer 2000 FT-IR and a high temperature vacuum cell. For vacuum creation, turbomolecular vacuum pump set-up from Pfeiffer Vacuum was used. The measured samples were prepared as self-supporting wafers without any diluting materials. Wafer weights of 5.5 – 16.0 mg were used in the successful measurements. Before placing the pellets into the vacuum cell, background for each of the measurements was obtained under vacuum in room temperature. Each wafer was dried prior the actual measurement of the spectra by heating them under vacuum to 400 °C with a ramp of 5 °C/min, temperature to which the wafers were left to dwell for 1h. West 6400 was used as the temperature controller for the cell heating. After the dehydration step, samples were cooled down with water cooling, under vacuum to 150 °C at which temperature the spectra were collected. Scan range of 4000-1000 cm^{-1}, scan interval of 1.0 cm^{-1} and resolution of 4 cm^{-1} were used with accumulation of 20 for the measured spectra.

N_2 physisorption characterizations were performed at an external laboratory and the results received are presented within this study as received. For total surface area of the samples Brunauer-Emmett-Teller (BET) method was employed and the external and internal surface areas and micropore volumes were obtained via the t-plot method. No further details of the performed N_2 physisorption measurements were received with the obtained results.

2.3 Steaming set-up

To attain dealumination of the framework of the synthesized Cu-SSZ-13, the samples were steamed with an in-house set-up which is schematically presented in the Figure 4. For the Cu-SSZ-13 samples further to be impregnated, two batches of Cu-SSZ-13 were steamed at 730 °C, one with mass 3 133 mg and the other using mass 3 615 mg. For other steaming temperatures of 610 °C, 690 °C and 820 °C used Cu-SSZ-13 samples originate from different batches. Flows of 200 ml/min of N_2 and 53 g/h of liquid water were used as the input feed. Brooks 5850S Mass Flow Controller was used to regulate the N_2 flow while Brooks Flomega Liquid Flow Controller was used for liquid water flows. The flows of both flow controllers were operated manually using Brooks 0154 Mass Flow Microprocessor control box and the flows were turned off by using a standard commercial power-off timer attached to the power source of the control box. The liquid water was vaporized to steam in the vaporizer, which was set to the temperature of 120 °C. The steam was then mixed with the N_2 flow and led through a pipeline heated to 120 °C, to the quartz reactor where the sample was set on a semipermeable holder. Temperature controllers used were a West 3810 for the vaporizer and a

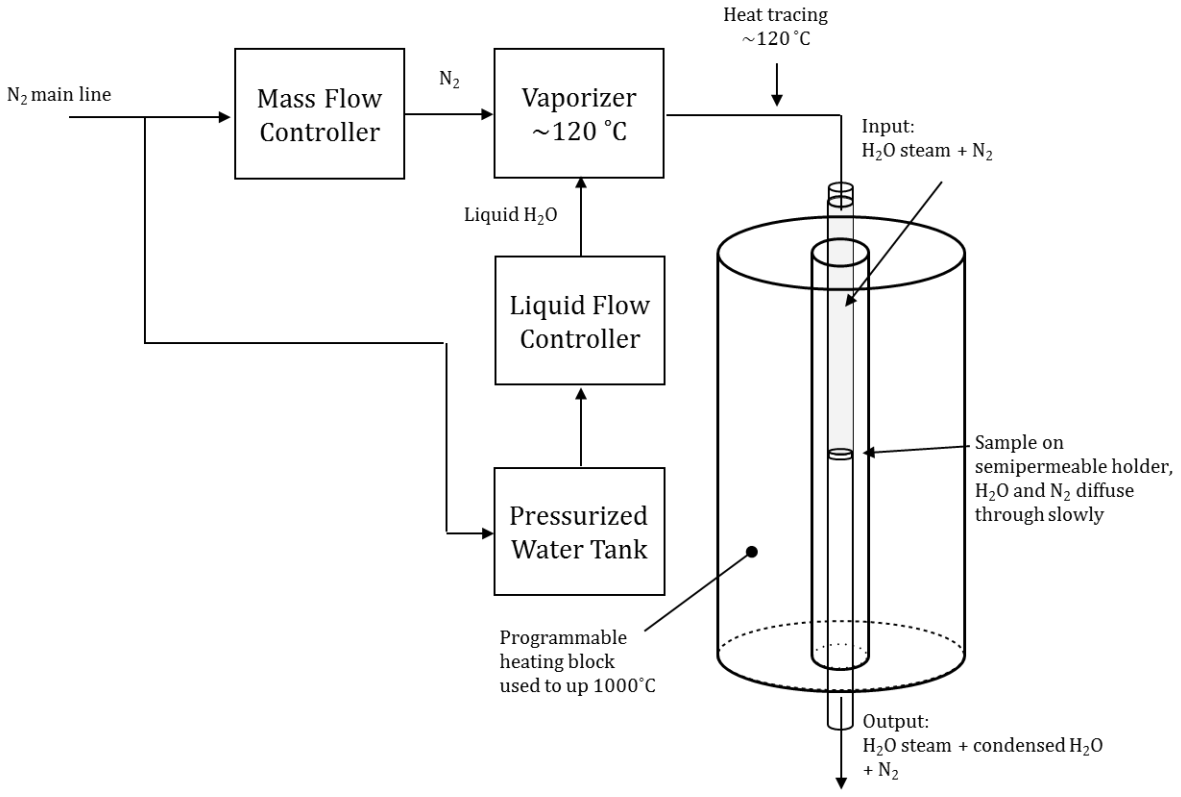

Figure 4: A schematical presentation of the set-up used to steam the Cu-SSZ-13 samples.

West 8100 for the pipeline heat tracing. The whole reactor tube was heated with a programmable heating block, equipped with temperature controller Nabertherm P330, up to temperatures of 610 °C, 690 °C, 730 °C or 820 °C depending on the sample used. The time under water steam was in total 16h of which 13h at the highest temperature, for each sample, as according the heating program devised by Moliner *et al.*[34] The heating program used is reproduced in the Appendix Figure B-4.

2.4 Catalytic testing set-up

To test the catalytic activity of the prepared samples, an in-house catalytic set-up was used. The set-up is depicted in Figure 5. A non-impregnated non-steamed Cu-SSZ-13 sample was tested as a reference sample for later comparison to the deactivation of the steamed only sample and steamed and subsequently Ca, P, Pt or Zn impregnated samples. Catalytic testing was done under plug flow conditions with the assumption of steady-state reaction conditions. Steady-state conditions were assumed as soon as gas output concentrations measured were constant. Measuring the output gas mixture was done continuously with Hiden Analytical HPR-20 QIC Mass Spectrometer (MS) and

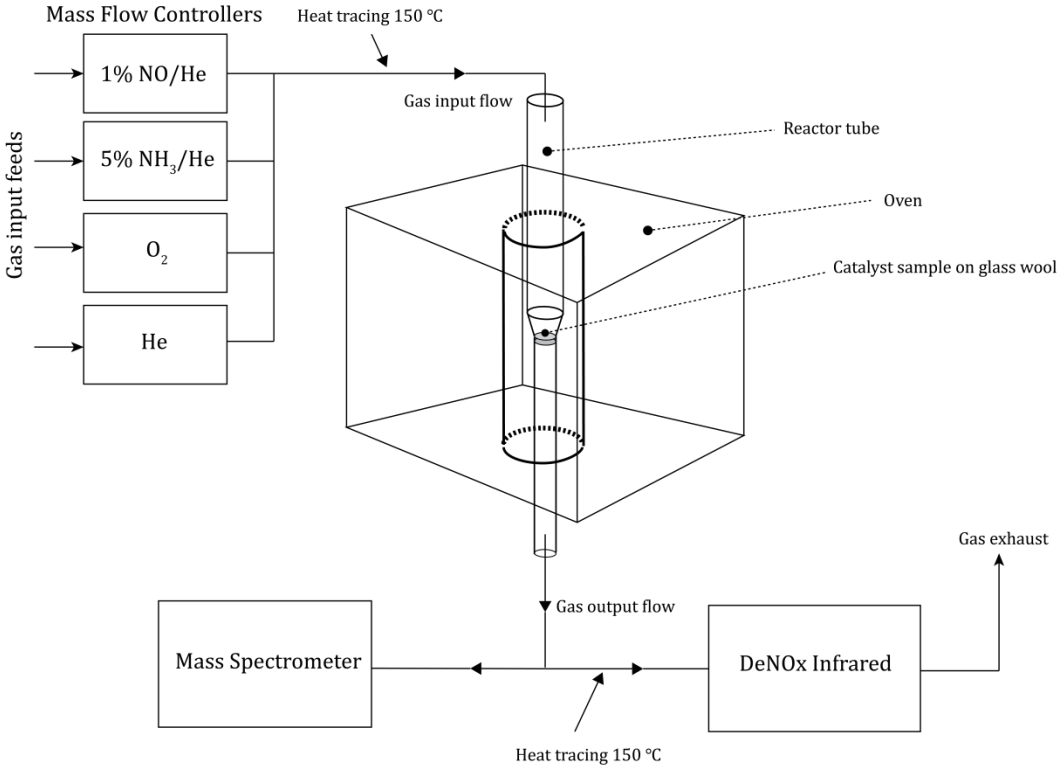

Figure 5: A schematical presentation of the set-up used to test the samples in NH_3-SCR reaction.

Perkin Elmer Spectrum One FT-IR Infrared Spectrometer (which is from now on now dubbed as the $DeNO_x$ IR for distinction to vacuum IR characterizations mentioned earlier). For the $DeNO_x$ IR, a non-heated gas cell with KBr windows with beam path length of about 5 cm, was used. The $DeNO_x$ IR spectra were collected over a range of 4000-700 cm^{-1} with scan speed of 0.5 cm^{-1}/s using resolution of 8 cm^{-1} and accumulations of spectra was set to 40. These settings resulted in scan time interval of 44 s. For each experiment performed, the $DeNO_x$ IR background scan was performed from the dried sample, i.e. when no more desorption of water was observed from the sample in the MS spectrum. All the values reported in the present paper are calculated as based on the DeNOx IR measurements, as the MS measured values were found to be highly depended on the used calibration line, and therefore, giving unreliable measured absolute gas output concentrations.

Sample size of 200 mg was used for the reference calcined Cu-SSZ-13 sample and for the lower density steamed only and steamed and subsequently impregnated samples, 180 mg of sample were used each to gain identical Gas Hourly Space Velocity (GHSV) of 67 500 h^{-1} for all the experiments. The samples were sieved to have a particle size range of 0.450-0.125 mm and then inserted to a quartz reactor tube where the sample was kept on place with a plug of glass wool. The reactor tube was then inserted inside the oven used for heating the samples and the reactor tube was furthermore connected to the gas line. The gas line from Mass Flow Controller outputs up to the $DeNO_x$ IR gas cell was heated to 150 °C using heat tracing covering the pipeline and a West 6100+ temperature controller. Input gas feed mixture of 896 ppm of NO and 945 ppm of NH_3 with 5% O_2 in the feed and helium as fill gas, was used to simulate the Standard SCR reaction (1) for each catalytic test performed. Brooks 5850 Mass Flow Controllers were used for each gas, and the gas flows were set manually using the LabView software and also, the temperature in the oven used to heat up the samples for the catalytic tests, was controlled manually via interface on the West 6100+ temperature controller. In Appendix Table B-1 is described the gas flow and temperature program used for the catalytic tests. The equation (4) was used to calculate the NO conversions;

$$\text{NO conversion } [\%] = \frac{NO_{in} - NO_{out}}{NO_{in}} \times 100 \qquad (4)$$

that is, the calculated NO conversion only considers the amount of removed NO from the stream regardless the reaction products (i.e. equation 4 ignores the reaction selectivity). To take into consideration the reaction selectivity, NO_2 and N_2O concentrations in the output gas feed were calculated. As N_2 is not IR active, calculation of the reaction selectivity as a product ratio, is not possible with using solely the $DeNO_x$ IR as the measurement method without using any

approximations. Therefore only the NO_2 and N_2O concentrations (as ppms) are reported and used to discuss the selectivity for the reactions.

To convert the measured $DeNO_x$ IR absorptions to the output gas concentrations, coefficients determined by the previous users working with the set-up were used. In short, each measured output gas was followed with a chosen wavenumber on which the species is known to absorb in the $DeNO_x$ IR spectrum and preferentially the wavenumber was chosen from such range that the absorption does not overlap with any other absorption from other species. The absorptions measured on the specific wavenumber were then converted to the output gas concentrations by multiplying the measured absorptions with predetermined coefficients, i.e. using the Beer-Lambert law.[35] The coefficients used were previously determined for each measured gas by flowing through the $DeNO_x$ IR cell a known concentration of the gas, then the calculating the absorption coefficient using the known concentration and the measured absorption.

3 RESULTS & DISCUSSION

The UV-Vis, IR, XRD and N_2 physisorption results, where obtained, are presented and discussed by the treatment method in the following sections. The results after calcination of the synthesized Cu-SSZ-13 are discussed in section 3.1. In following section 3.2, observed effects due to the steaming treatment of samples are presented. The effect of impregnation on the steamed samples is discussed in section 3.3. In section 3.4, the last section of the chapter, the catalytic test results for the calcined, steamed and steamed and impregnated samples are discussed.

To follow changes in the crystalline structure of the samples, XRD was used. The XRD patterns obtained for calcined Cu-SSZ-13 and for Cu-SSZ-13 samples steamed at 610 °C, 690 °C, 730 °C and 820 °C are presented in Figure 6. As based on the XRD patterns in Figure 6, the steaming temperature at 730 °C was chosen to serve as the steaming temperature for the to-be-impregnated samples, as some loss in the catalyst framework crystallinity was achieved without completely destroying the catalyst framework. To compare the effect of the impregnation on the crystalline structures, XRD patterns for calcined Cu-SSZ-13 sample, sample steamed at 730 °C and samples steamed at 730 °C and subsequently impregnated with Ca, P, Pt or Zn, are presented in Figure 9.

The UV-Vis spectra to probe the electronic states of the species present in the prepared Cu-SSZ-13 zeolites are reported for samples steamed at 610 °C, 690 °C, 730 °C or 820 °C, in Figure 7, and for sample steamed at 730 °C and subsequently impregnated with either Ca, P, Pt or Zn the spectra are presented from Figure 10 through Figure 13.

The IR spectra were obtained for the Cu-SSZ-13 samples to follow the changes in the OH groups on the Cu-SSZ-13 surface upon steaming treatment. The IR spectra for samples steamed at temperatures of 610 °C, 690 °C or 730 °C and for a reference, IR spectra from a calcined only Cu-SSZ-13 sample was also obtained. Each IR sample was first dehydrated at 400 °C in vacuum for 1h and the measurement of the spectra were performed after cooling down the samples to 150 °C, under vacuum, as described in the experimental section prior. Obtaining the IR spectra for the Cu-SSZ-13 sample steamed at 820 °C was not successful as it was not possible to form a self-supporting wafer from the sample. The IR spectra obtained were normalized by the used wafer weight and the normalized spectra are presented in Figure 8. The IR spectra are shown for the region of 3800 – 3300 cm^{-1} where the absorptions due to OH stretching vibrations attached to the different sites over the zeolite framework or extra-framework Al are known to reside.[36,37]

N_2 physisorption measurements were performed by an external laboratory for the Cu-SSZ-13 sample steamed at 730 °C and for samples steamed at 730 °C and subsequently impregnated with Ca, P, Pt or Zn. As a reference, N_2 physisorption results for a calcined only H-SSZ-13 from a study by Sommer *et al.,*[38] was used. N_2 physisorption tests were used to obtain the BET surface area (the total surface area of the sample), the external and internal surface areas and the micropore volumes of the samples. Values received from the external laboratory are reported in the Table 1 as received.

3.1 Calcined samples

In Figure 6 is presented the XRD pattern obtained for the calcined Cu-SSZ-13 reference sample. The calcined only Cu-SSZ-13 sample was identified to possess SSZ-13 (CHA) framework structure,[39] and the additional peaks resulting from Co K_β radiation were assigned successfully with the DIFFRACplus software, i.e. the synthesis of crystalline SSZ-13 framework was successful.

From the UV-Vis spectrum in Figure 7 it can be seen for the non-steamed Cu-SSZ-13 sample, after calcination, that an intense absorption at the wavenumber 48 500 cm^{-1} is present and a less intense, broader absorption is peaking at 11 500 cm^{-1}. The 48 500 cm^{-1} peak can be assigned to the charge transfer band $O_{lattice} \rightarrow Cu^{2+}$, i.e. for charge transfer from zeolite lattice oxygen to an isolated Cu^{2+}-ion,[12,16,40–42] while the broad absorption at 11 500 cm^{-1} is due to a d-d transition in an Cu^{2+}-ion.[12,16,41,42] The small shoulder in the calcined only Cu-SSZ-13 absorption at about 34 400 cm^{-1} can either be associated as a part to the $O_{lattice} \rightarrow Cu^{2+}$ charge transfer band,[41] or is due to the zeolite matrix absorption edge.[43] Sharp absorptions below 7300 cm^{-1} are in the Near Infrared range (NIR) and are due to structural vibrations of the zeolite structure. No additional absorptions for mono(μ-oxo) dicopper at 22 700 cm^{-1} or Cu^{+}-ions at around 34 000 cm^{-1} are present,[32,42,44] confirming that the ion-exchange had indeed been successful and solely Cu^{2+}-ions were introduced to the SSZ-13 framework structure as the charge compensating cations. The intensity differences observable in the absorptions in Figure 7 between the samples are due to the fact that the samples originate from different parents and precise compositions (e.g. Cu-loading and Si:Al ratio) of the samples might not be identical.

The IR spectrum of the calcined Cu-SSZ-13 sample in Figure 8 shows three distinctive peaks at wavenumbers 3733 cm^{-1}, 3608 cm^{-1} and 3585 cm^{-1}, and less intense and broad absorptions at 3704 cm^{-1} and 3502 cm^{-1}. The mentioned IR peak positions agree well with H-SSZ-13 zeolite as compared to a study by Smith *et al,*[45] The peaks 3608 cm^{-1} and 3585 cm^{-1} are due to two different bridging hydroxyl groups forming the Brønsted acid sites on the SSZ-13 framework.[38,45] The peak at 3733

cm^{-1} could be assigned to the OH-groups in the isolated silanol groups (i.e. non-hydrogen bonded silanol group) which reside on the internal surface (in the pores) of the zeolite framework.[46,47] The 3704 cm^{-1} absorption is most likely an hydrogen bonded or vicinal silanol group present at framework defect sites.[37,38,46] Another broad adsorption seen in the calcined Cu-SSZ-13 sample around 3502 cm^{-1} can be assigned for hydroxyl nests which are present due to synthesis defects in the calcined only Cu-SSZ-13 sample.[37,38,43,46] As Sommer *et al.* have discussed, the simultaneous presence of the absorptions at 3704 cm^{-1} and 3502 cm^{-1} in their calcined H-SSZ-13 sample seem to be indicative of defect sites in the framework due to synthesis.[38]

3.2 Steamed samples

As can be seen from the XRD patterns presented in Figure 6, increasing the steaming temperature gradually from 610 °C to 820 °C causes loss of definition in the XRD patterns which signifies loss of crystalline structure of the Cu-SSZ-13 zeolite. Similar results have been obtained by Schmieg *et al.* in their experiments for unspecified CHA-zeolite.[6] The loss of crystallinity and degrading framework is due to progressing dealumination process in which the Al is removed from the framework until complete collapse of the framework.[6] Also, the XRD results obtained within this study compare well with Moliner *et al.*,[34] with similar method and steaming conditions of the Cu-

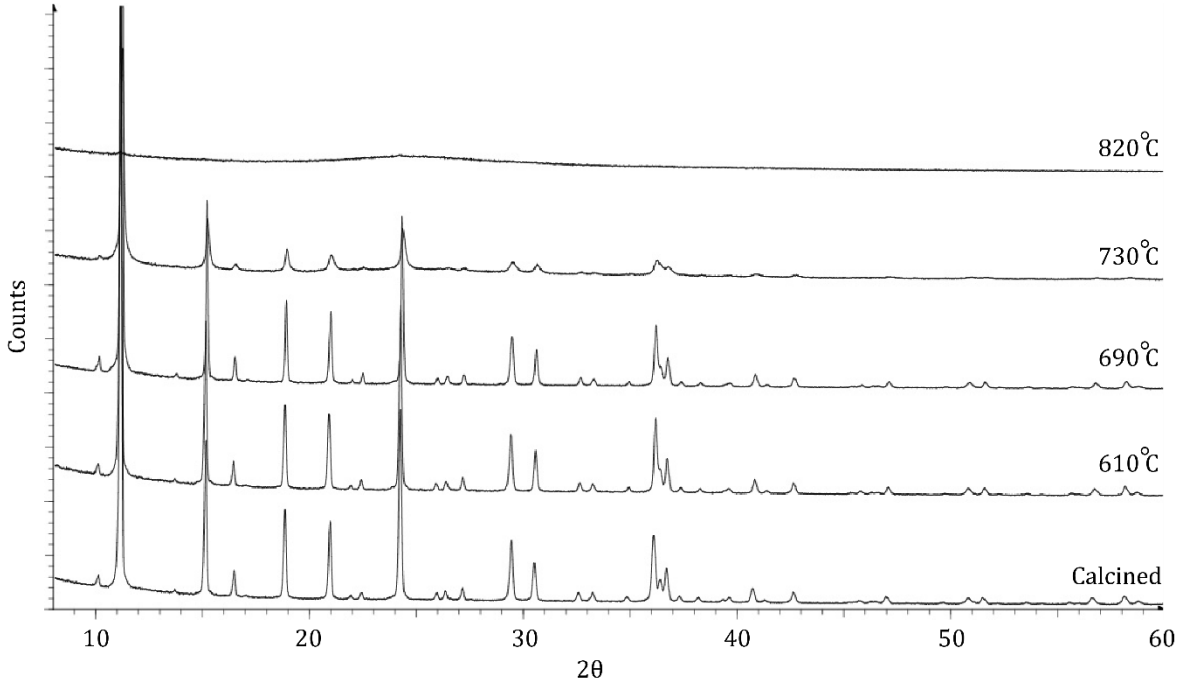

Figure 6: The XRD patterns obtained for calcined reference sample of Cu-SSZ-13 and for Cu-SSZ-13 samples steamed at temperatures of 610 °C, 690 °C, 730 °C and 820 °C for 13h.

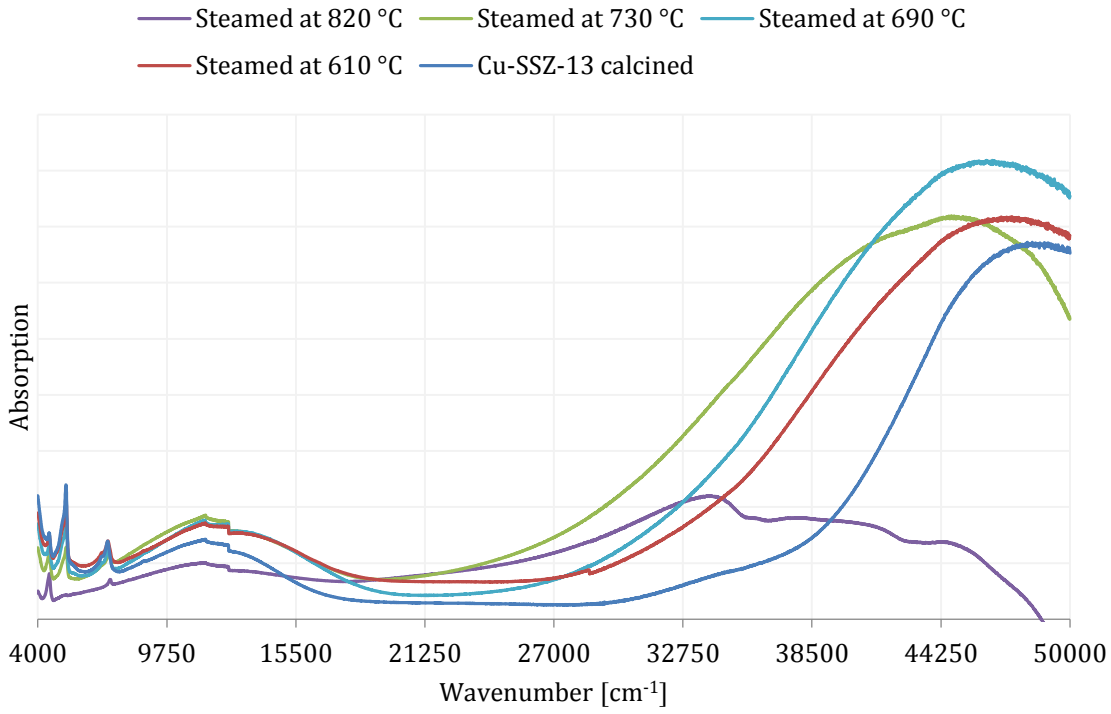

Figure 7: The UV-Vis spectra for calcined Cu-SSZ-13 sample and for Cu-SSZ-13 samples steamed at 610 °C, 690 °C, 730 °C or 820 °C for 13h. The used steaming program shown in the Appendix Figure B-4 and the used program is devised by Moliner *et al.*, from reference 34.

SSZ-13. To note here, as Moliner *et al.* have shown in their study, Cu-SSZ-39 (AEI framework) shows even more resiliency towards dealumination than Cu-SSZ-13 and could be another good zeolite catalyst for NH_3-SCR.[34]

As regarding the effect of the steaming temperature on the UV-Vis spectra, two main effects can be observed in Figure 7. The Cu^{2+} charge transfer band swifts progressively towards lower wavenumbers, from the 48 500 cm^{-1} of the calcined only sample to the 45 000 cm^{-1} for the sample steamed at 730 °C, as the steaming temperature is increased. Additionally, the absorption band starting from 36 600 cm^{-1} progressively broadens to start from 22 700 cm^{-1} as the steaming temperature increases. The sharp drop in each spectrum in Figure 7 (as well as in any spectrum obtained in the study) at 12 000 cm^{-1} is due to changing light source in the used UV-Vis instrument.

The first effect, the shifting Cu^{2+} charge transfer band is due to changing electron donor strength of the SSZ-13 framework. As the Al is removed from the zeolite framework due to the steaming treatment, the Si:Al ratio of the framework increases, leading to decreased donor strength

of the zeolite framework which results in a shift of the Cu^{2+} charge transfer band towards lower wavenumbers.[43,48]

The second effect, the broadening peak, is due to formation of copper oxides. As the increasing steaming temperature progressively degrades the SSZ-13 framework (see the XRD patterns in Figure 6) by removing the Al from the zeolite framework, therefore less anchoring sites Cu^{2+} ions have and more of Cu^{2+} ions are prone to sintering and towards formation of clustered copper oxides. The formed copper oxides absorb within the range of about 27 000 – 37 500 cm^{-1} and the position of the absorption is also related to the copper oxide cluster size.[43] Therefore, it can be interpreted from the UV-Vis spectra in Figure 7, as the steaming temperature is increased, increasing amount of Cu^{2+} ions are clustered to copper oxides due to lost or distorted framework Al which results in the sintering effect of the Cu. The appearance of the slight second peak at 41 500 cm^{-1} is also due to the formed copper oxides and the overlapping of the copper oxide absorption bands and the Cu^{2+} charge transfer band.

The d-d transitions for the Cu^{2+} ion at 11 500 cm^{-1} in Figure 7 remain rather same without any clear connection to the steaming temperature, indicating that no now species giving d-d transitions or neither new coordination environments for the Cu^{2+} were formed due to steaming treatment, as the location of the Cu^{2+} d-d transition reflects the coordination environment of the Cu^{2+} ion.[42,43]

According to the UV-Vis spectra for the steamed samples, Cu clustering starts already at the lowest steaming temperature of 610 °C while XRD pattern (Figure 6) for the same steaming temperature does not show any significant loss in the sample crystallinity. However, as will be discussed shortly, from the IR spectra (Figure 8) it can be seen that the Brønsted acid sites on the bridging hydroxyl groups are mostly lost already after steaming at 610 °C, i.e. Al seems to be partially distorted or removed from the framework which mostly likely causes the loss of anchoring sites for the Cu^{2+} ions also, resulting in the copper clustering which can be observed on the UV-Vis.

Finally to mention regarding the UV-Vis spectra of the samples steamed progressively at increasing temperature, the UV-Vis spectra of sample steamed at 820 °C suggests the same event as the XRD pattern in the Figure 6 for the same sample: loss of crystalline structure as no charge transfer band at region 43 300 – 48 500 cm^{-1} can be seen anymore, signifying that there are no more framework locations for the Cu^{2+} ions to reside as an isolated ion and a mixture of copper oxides are formed.

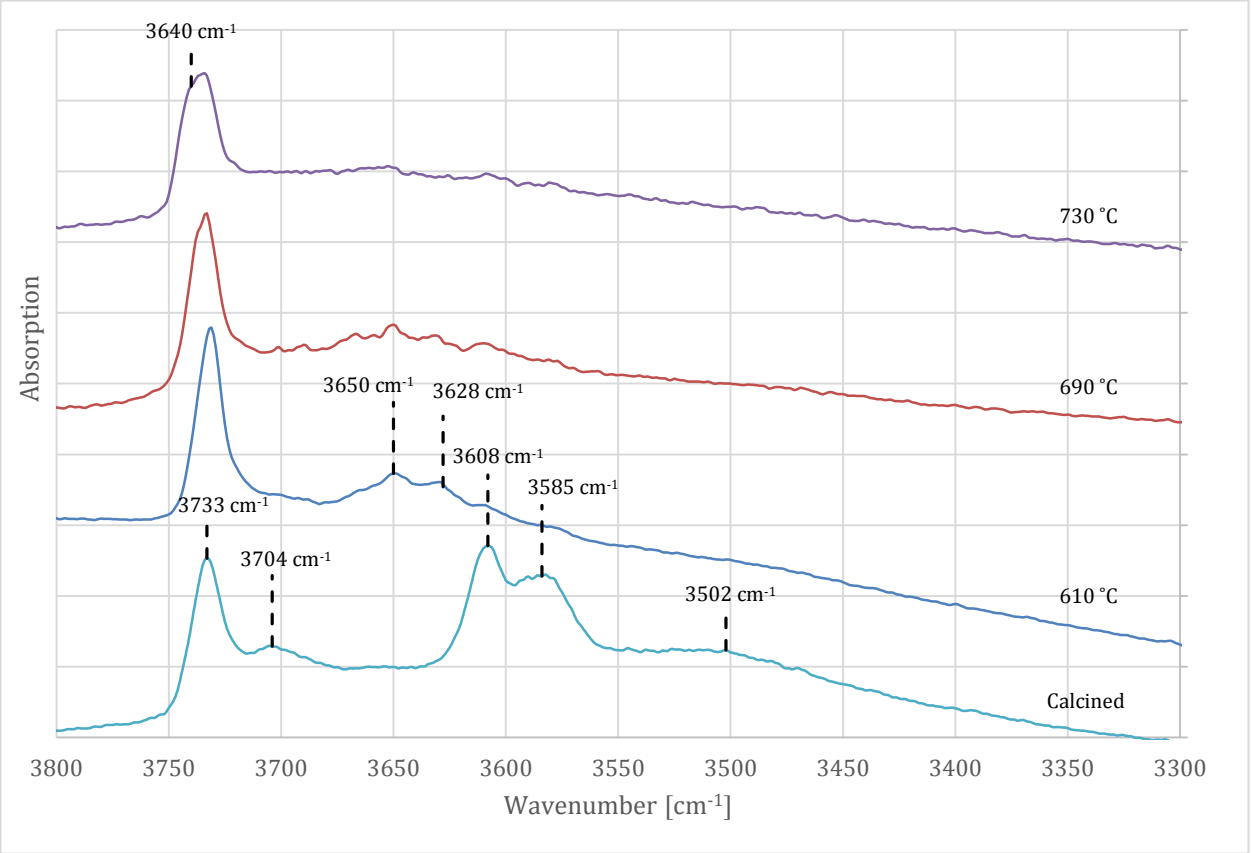

Figure 8: The IR absorption spectra acquired for the range of 3800-3300 cm^{-1} where absorptions due to OH groups can be observed. Spectra are presented for calcined Cu-SSZ-13 and for CU-SSZ-13 samples steamed for 13h at 610 °C, 690 °C or 730 °C. The samples were first dehydrated at 400 °C and then cooled down to 150 °C (under vacuum) at which temperature the spectra were measured. Each spectrum is normalized by the used wafer weight. No IR spectra could be obtained for Cu-SSZ-13 sample steamed at 820 °C for 13h due to instability of the formed wafer for the IR measurement.

In the IR spectra of the steamed samples (Figure 8), appearance of absorption peaks at region of 3620-3660 cm^{-1} for the sample steamed at 610 °C and their progressive disappearance with increasing steaming temperature is seen. Also, disappearance of the absorptions at 3704 cm^{-1}, 3608 cm^{-1}, 3585 cm^{-1} and 3502 cm^{-1} already at steaming temperature of 610 °C is observed as compared to the calcined only sample. As the last feature to note from the IR spectra presented in Figure 8, broadening of the peak at 3733 cm^{-1} towards 3740 cm^{-1} takes place progressively with increasing steaming temperature.

The new absorptions formed within the range of 3620-3660 cm^{-1} after steaming at 610 °C can be assigned to the formation of partially distorted framework Al to which OH groups are coordinated.[23,38,47,49] The formation of partially distorted Al explains the loss of absorption intensity associated to the presence of the Brønsted acid sites at 3608 cm^{-1} and 3585 cm^{-1}. As the framework

Al is lost or distorted, the bridging hydroxyls groups are removed,[20,23] which is seen as lost absorption at 3608 cm^{-1} and 3585 cm^{-1} upon steaming (Figure 8). As the steaming temperature is progressively increased up to 730 °C, a loss of absorption is also seen in the region 3620-3660 cm^{-1} assigned for the OH groups in the partially bound framework Al. The absorption loss with increasing steaming temperature could be explained to be due to partially distorted Al species first forming extra-framework Al species which then subsequently condense to Al phases, which do not incorporate any OH groups and are therefore invisible over the IR range shown in the Figure 8.[23]

The IR absorption at around 3780 cm^{-1}, absorption which is associated usually to OH group on extra-framework Al,[23,46,47] is not seen for some reason in this case even though such adsorption might be excepted to be seen due to progressing dealumination process. Such absorption has been seen for other zeolites as the dealumination progresses,[23,47,49] but not for H-SSZ-13 for some unknown reason.[38] Perhaps a possible reason could be that the lowest used steaming temperature of 610 ˚C could already be high enough to cause the condensation of the Al species or perhaps, for SSZ-13 the Al could have higher tendency to form condensed extra-framework Al species than with the other zeolite frameworks. However, the lack of absorption at 3780 cm^{-1} due to OH groups on extra-framework species cannot be adequately answered here and further studies would be needed to answer the question.

Loss of absorption intensity at the hydrogen bonded OH groups or vicinal silanol groups on defect site at 3704 cm^{-1} and hydroxyl nests at 3502 cm^{-1} can be observed upon steaming as compared to the calcined only sample (Figure 8). The defect sites in the framework should be the most susceptible starting points for the progressing structure degradation,[37] and the absorptions at 3704 cm^{-1} and 3502 cm^{-1} are indeed lost already at the lowest steaming temperature of 610 ˚C. As Kawai *et al.* and Sommer *et al.* have discussed,[24,38] as the zeolite framework degradation progresses, mesopores should be formed. As following an explanation given by Kawai *et al.*, upon progressing structure degradation the hydrogen bonds between silanol groups are broken as the silanol groups are too far away from each other on the formed mesopore walls, that no hydrogen bonding is possible.[24] Formation of the mesopores might then explain the loss of absorptions at 3704 cm^{-1} and 3502 cm^{-1}, both absorptions which could be due to hydrogen bonded silanols. Furthermore, the silanol groups at the mesopore walls should appear in the IR spectra as external isolated silanol groups within the range of 3740-3745 cm^{-1}.[24,37,46,47] As seen from the Figure 8, as the steaming temperature is increased, indeed broadening of the peak at 3733 cm^{-1} towards 3740 cm^{-1} is

observed, and the broadening at 3740 cm^{-1} might indicate formation of external silanol groups, as discussed.

For the sample steamed at 730 °C, N_2 physisorption measurements were performed in an external laboratory and the results are presented in the Table 1. As compared to the reference values for calcined only SSZ-13 framework, upon steaming at 730 °C, the BET total surface area drops from 704 m^2/g to 323 m^2/g, micropore surface area from 679 m^2/g to 288 m^2/g and micropore volume drops from 0.25 cm^3/g to 0.11 cm^3/g. Instead of decreasing, the external surface area (i.e. external surface of the SSZ-13 crystal and the surface which is not a micropore surface) is seen to increase from 25 m^2/g to 36 m^2/g. According to Sommer *et al.*, losses in the BET total surface area, micropore surface and volume can be explained with partial destruction of the SSZ-13 framework and the increase of the external surface is said to be due to formation of mesopores to the framework.[38] However, more research would be needed to confirm or disproof this assumption of mesopore formation, such as more systematic N_2 physisorption measurements for all the steamed samples to reveal possible trends in the developments in the catalyst surface areas upon steaming.

3.3 Impregnated samples

To determine the effect of the selected chemical species on the steamed Cu-SSZ-13 catalyst, samples of calcined Cu-SSZ-13 steamed at 730 °C and then subsequently impregnated with Ca, P, Pt or Zn using the Wet Impregnation method, were prepared. The precise preparation method was described earlier in the experimental section 2.1.

The effect of impregnation with Ca, P, Pt or Zn on obtained XRD patterns can be seen in Figure 9. For samples impregnated with either Ca or P, no extra peaks in the XRD patterns were present as compared to the non-impregnated Cu-SSZ-13 samples. For the Pt and Zn impregnated samples additional peaks appeared after impregnation with the chemical species. For Pt, the peaks marked with * (in Figure 9) were assigned to Pt^0,[50] and for Zn impregnation, peaks signed with # were found to originate from ZnO.[51]

Formation of metallic Pt^0, even though a relatively low Pt-loading of 2 wt-% was used, is most likely due to migration of the Pt precursor during the drying step at 120 °C in the calcination program (Appendix Figure B-3), during which most of the water solvent is removed from the zeolite pores.[19] When the $Pt(NH_3)_4(NO_3)_2$ precursor is solvated, $Pt(NH_3)_4^{2+}$ is formed. Due to the precursors positive charge it interacts poorly with the zeolite surface, from which the Al has been

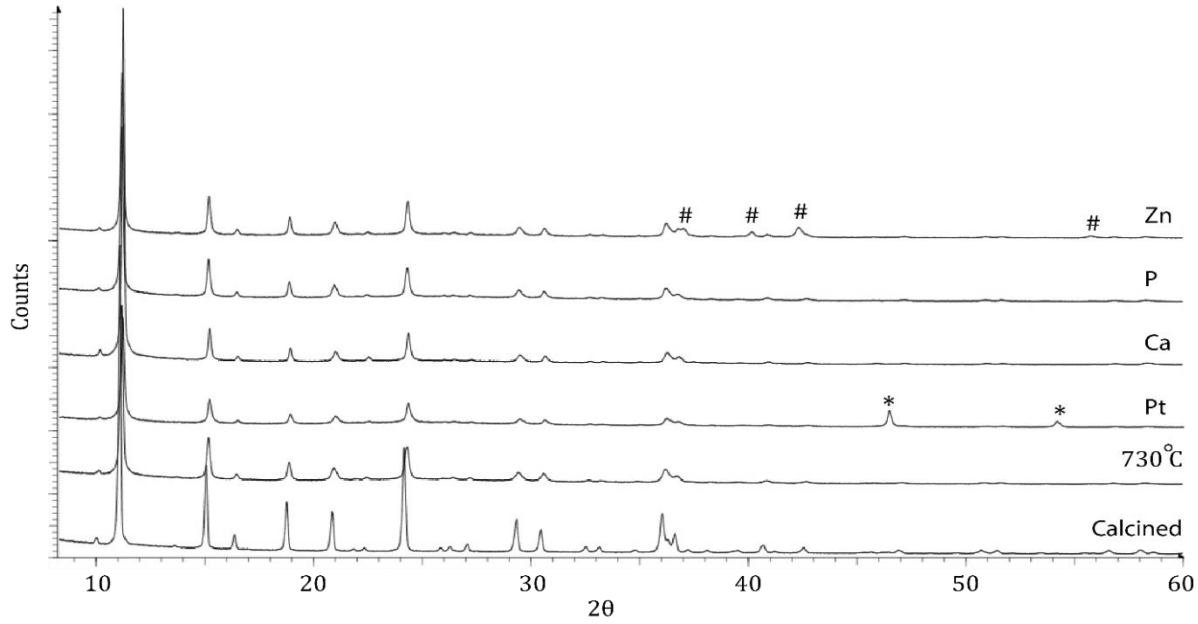

Figure 9: The XRD patterns obtained for calcined Cu-SSZ-13, for sample steamed at 730 °C for 13h and for Cu-SSZ-13 samples which were impregnated with either Zn, P, Ca or Pt after steaming treatment of Cu-SSZ-13 at 730 °C for 13h. In the Zn pattern; # marks peaks assigned for ZnO, in the Pt pattern; * marks peaks identified for Pt^0.

(mostly) removed with the prior steaming treatment, leaving a hydrophobic i.e. non-charged surface.[24] Therefore, the $Pt(NH_3)_4^{2+}$ migrates to the zeolite surface as carried by the water molecules during the drying step at 120 °C and the heating ramp in the used calcination program (see Appendix Figure B-3 for the used temperature program for calcination). Notably, as described earlier in the experimental section, a large amount of water was used during the Pt impregnation due to poor solubility of $Pt(NH_3)_4(NO_3)_2$, resulting in even higher likeness for migration of the precursor.[19] Formation of the Pt^0 is then due to tendency of the Pt^{2+}-ions to auto-reduce on the zeolite surfaces, even under calcining conditions i.e. with heat and O_2 atmosphere, if the original drying step has been too fast.[52] In this study, drying step was steady at 120 °C and the heating ramp used to raise the temperature to 120 °C was 2 °C/min, a total drying rate lower than 0.5 °C/min could have prevented the formation of the Pt^0 species.[52] Therefore, it seems that the Pt-precursor $Pt(NH_3)_4^{2+}$ may have migrated out of the zeolite pores to the sample surface during the drying step (during removal of water, that is) in the calcination program to form high local concentrations of Pt at the zeolite surface. Upon increased calcination temperature, the concentrated Pt precursors are then further auto-reduced to crystalline Pt^0 which can be observed in the XRD.

Formation of ZnO due to impregnation is most likely due to enrichment of the of the Zn on the zeolite surface, as observed by Tkachenko *et al.* in their X-ray Photoelectron Spectroscopy (XPS)

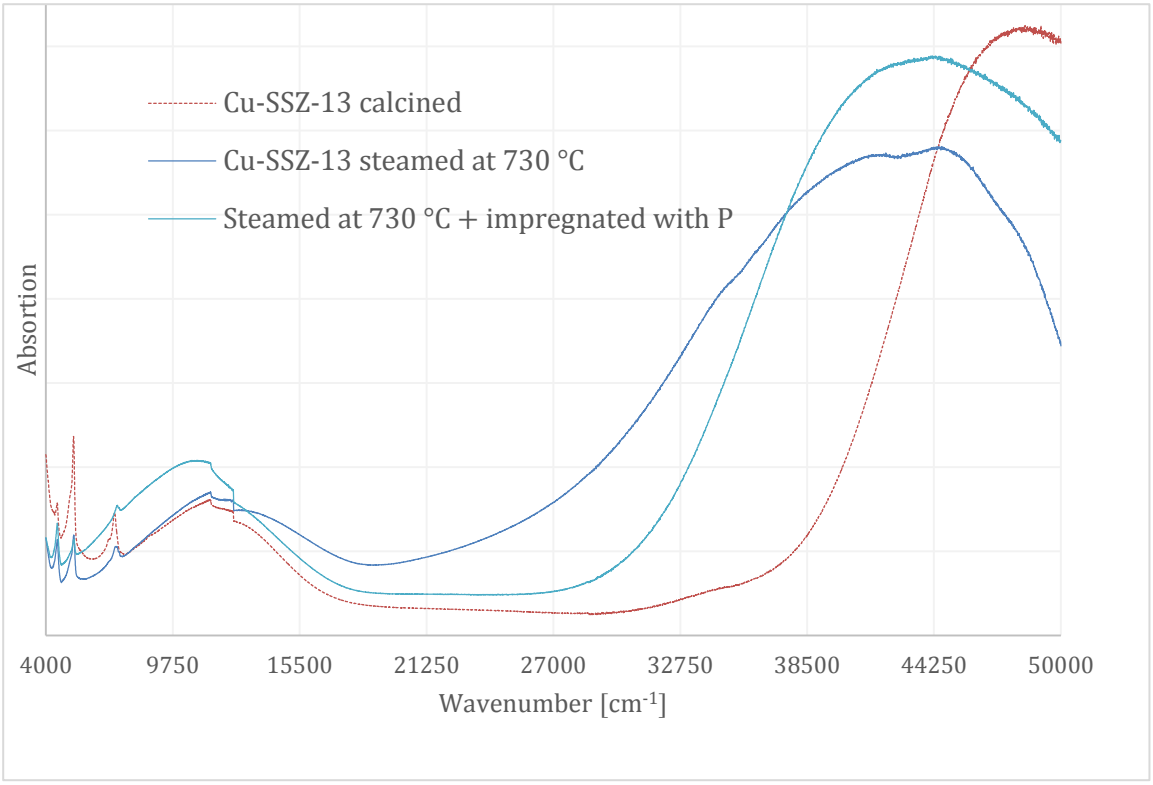

Figure 10: The UV-Vis spectra of calcined Cu-SSZ-13 sample, Cu-SSZ-13 sample steamed at 730 °C for 13h and Cu-SSZ-13 which has been steamed at 730 °C for 13h and then impregnated with P.

study of various zeolites impregnated with Zn.[53] Enrichment, in the present case, could be speculated to be due to same migration effect of the of the Zn precursor with water, as was described for the Pt, However, clear reasoning for the ZnO formation cannot be given with the available information.

The UV-Vis spectra for samples impregnated subsequently after steaming at 730 °C are presented in Figure 10 for P, Figure 11 for Pt, Figure 12 for Ca and in Figure 13 for the Zn impregnated samples. In these UV-Vis spectra, each steamed and impregnated sample is compared to its parent non-steamed Cu-SSZ-13 and steamed Cu-SSZ-13 sample. P, Zn and Ca samples originate from same parent Cu-SSZ-13 sample while Pt originates from different Cu-SSZ-13 parent, due to this, parent Cu-SSZ-13 samples show different absorption intensities between spectra of P, Zn, and Ca as compared to the UV-Vis spectrum of Pt. As regarding the steamed Cu-SSZ-13 samples shown in Figure 10 through Figure 13, the same discussion applies as presented previously in earlier sections for the steamed samples in Figure 7, but the precise absorptions are different as the samples are different.

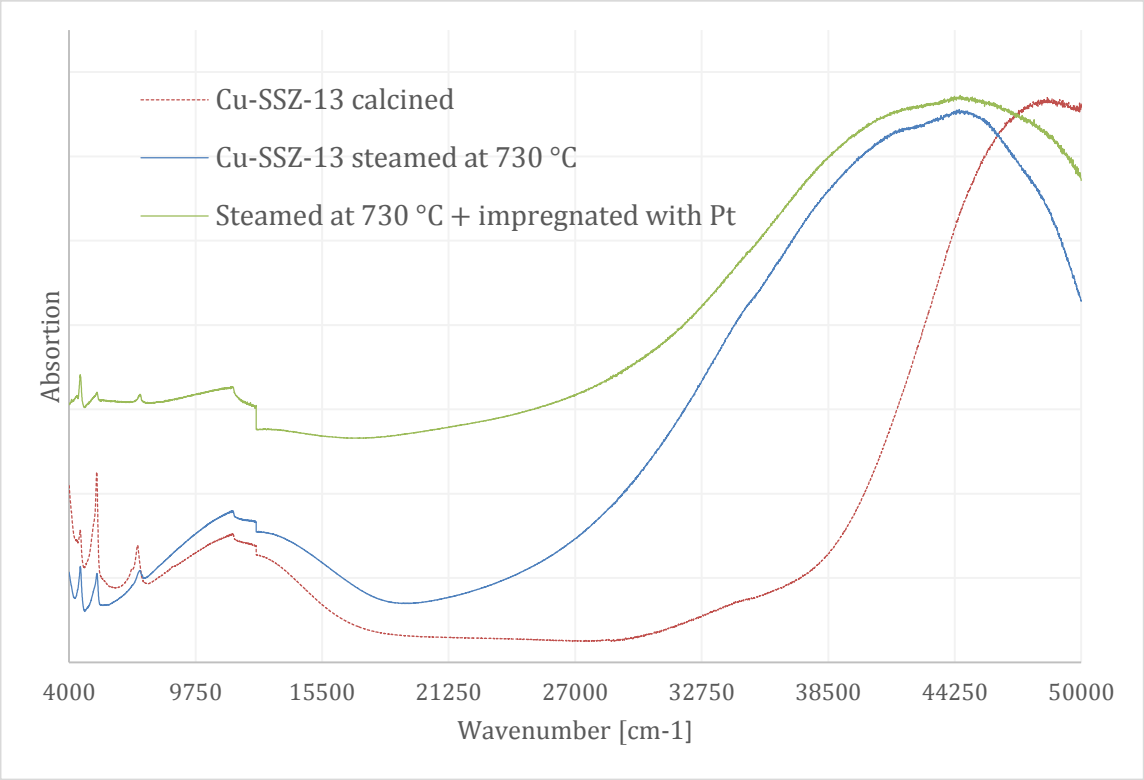

Figure 11: The UV-Vis spectra of calcined Cu-SSZ-13 sample, Cu-SSZ-13 sample steamed at 730 °C for 13h and Cu-SSZ-13 which has been steamed at 730 °C for 13h and then impregnated with Pt.

The UV-Vis spectrum of the steamed and subsequently P-impregnated sample is presented in the Figure 10. Two changes in the absorptions are imminent, as compared to the steamed-only parent sample. The d-d transition has broadened towards the lower wavenumbers, marking a change in the coordination environment of the Cu^{2+}-ion.[42] Also, the absorption introduced due to steaming and formation of clustered Cu-oxide species has lessened, absorption starting now from about 28 000 cm^{-1} instead of the 21 500 cm as were for the steamed only sample. At 44 250 cm^{-1}, new and uniform peak was formed instead of the twin-peak absorption for the steamed Cu-SSZ-13 sample.

The newly formed broad absorption peak, starting from about 28 000 cm^{-1} and peaking at 44 250 cm^{-1} could be due to a newly formed phosphate species.[54,55] Also, as Benarafa *et al.* observed in their study of calcium copper phosphates, d-d transitions for Cu^{2+} when being part of a phosphate structure, are at around 10 500 cm^{-1}, which could explain the d-d transition absorption broadening observed here.[56]

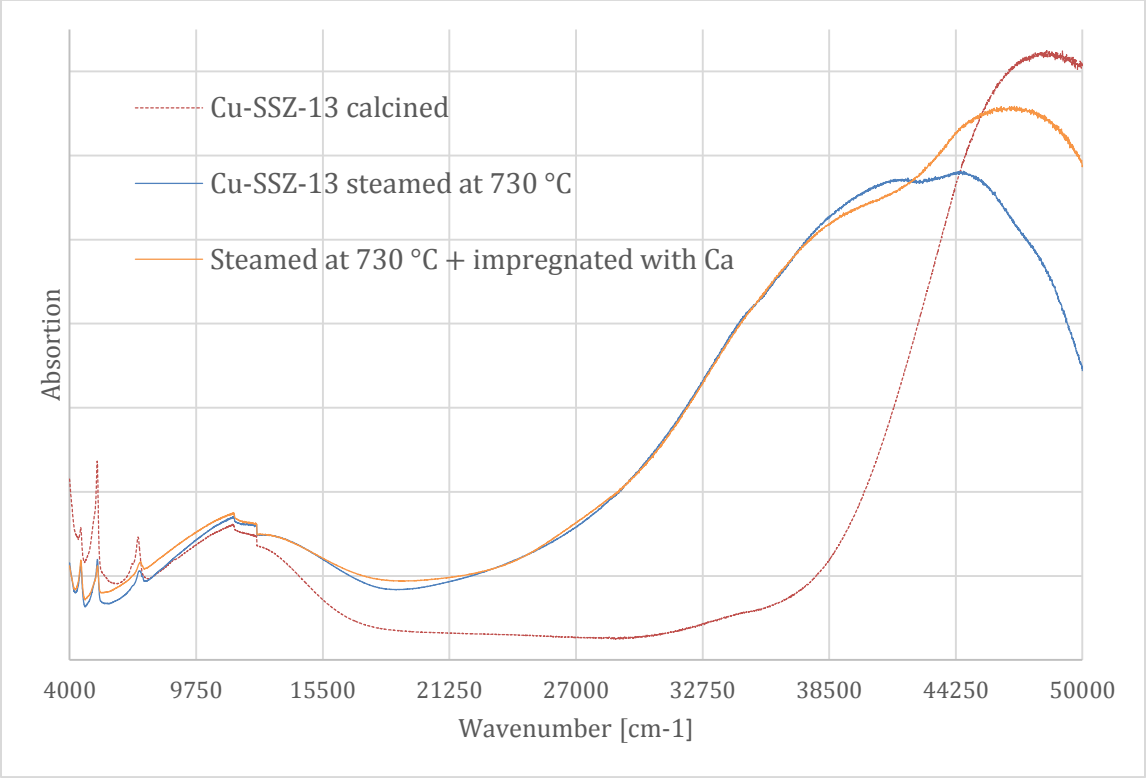

Figure 12: The UV-Vis spectra of calcined Cu-SSZ-13 sample, Cu-SSZ-13 sample steamed at 730 °C for 13h and Cu-SSZ-13 which has been steamed at 730 °C for 13h and then impregnated with Ca.

As $(NH_4)_2HPO_4$ was used as the precursor in the P impregnation and the Cu oxides were introduced to the zeolite surface due the prior steaming treatment, it could be possible that a copper phosphate species was formed during the P impregnation and the subsequent calcination step. Formation of Cu^{2+}-ion containing crystalline copper phosphates from CuO and $(NH_4)_2HPO_4$ has been shown to happen at 750 °C by Bamberger *et al.*[57] Therefore, it could be suggested that addition of $(NH_4)_2HPO_4$ might have led to a reaction with the Cu-oxides on the steamed Cu-SSZ-13 in which new copper containing species, an unspecified copper phosphate could have been formed. This could explain all the observed changes in the UV-Vis spectra for the P impregnated samples, the broadening d-d transitions as Cu^{2+} could be associated to a new coordination environment with the phosphate, loss of absorption due to Cu-oxides as the oxides could have been a reagent for the copper phosphate formation and rise of new broad absorption similar in shape to what has been observed for phosphates in other studies.[54,55] However, this is rather speculative as the temperature used here during the calcination treatment was at highest 550 °C nor additional crystalline structures were seen in the XRD upon P impregnation, and for this matter more

characterization results would be needed to confirm or dismiss the possible formation of copper phosphates.

The UV-Vis spectrum of the Pt-impregnated sample is presented in the Figure 11. The higher overall absorption of the steamed and Pt-impregnated Cu-SSZ-13 is due to its grey color which causes in overall increased absorption, as compared to the light green color of the steamed Cu-SSZ-13. Besides overall higher absorption, no distinctive changes are notable in the Pt-impregnated sample as compared to the steamed only Cu-SSZ-13. The d-d transition at 11 500 cm^{-1} remains the same as well as the twin-peak, the peak associated to copper oxides at 41 800 cm^{-1} and the another related to Cu^{2+} charge transfer at 45 000 cm^{-1} are also observable at the Pt impregnated sample. The grey color introduced to the Pt impregnated catalyst is due to formation of metallic Pt^0.[52] Similar, no distinctive features showing UV-Vis spectrum for Pt^0 containing zeolite, have been previously observed by Roldan *et al.* for calcined samples of Pt-Beta.[58] Therefore, the UV-Vis spectrum can be taken to agree with the XRD pattern for the same sample in Figure 9 and the species introduced on the catalyst is indeed Pt^0.

For Ca-impregnated Cu-SSZ-13, the UV-Vis spectrum is presented the Figure 12. After impregnating the steamed Cu-SSZ-13 with Ca, an intense absorption at 47 000 cm^{-1} on the charge transfer region appears. The new absorption at 47 000 cm^{-1} is most likely due charge transfer $O_{lattice} \rightarrow Ca^{2+}$ i.e. from zeolite lattice oxygen to the newly introduced Ca^{2+}-ion.[56] As the sample has been previously steamed removing the Al-atoms from the framework, and consequently abolishing the zeolite from its framework ion-exchange sites, arises a question what might be the site for the Ca^{2+}-ions to reside. An option could be the hydroxyl nests created on the framework defect sites upon steaming, as discussed by Roldan *et al.*[58] However, as discussed in the earlier section related to IR spectra of the Cu-SSZ-13 steamed at 730 ˚C, no hydroxyls nests or defect sites might be present or at least not seen in the IR spectrum for the sample. Also, Kawai *et al.* have deemed the hydroxyl nests to be highly unreactive and hydrophobic (i.e. uncharged),[24] making them unlikely to react with the positively charged Ca^{2+}. Regarding the rest of the spectra in Figure 12 besides the appeared absorption at 47 000 cm^{-1}, after the Ca impregnation as compared to the steamed catalyst; no changes can be seen and the spectra are nearly identical. The possible presence of the CaO, as a possible product present after calcination of the Ca-impregnated catalyst, is not likely to be seen in the UV-Vis spectra as CaO is poorly absorpting in the UV-Vis region,[59] and no sign of any diffraction peaks assignable to the CaO were seen in the XRD patterns in the Figure 9. Therefore,

according to the Ca-impregnated UV-Vis spectrum of the steamed Cu-SSZ-13, at least some Ca^{2+}-ion seems to be present but their location remains unknown.

With the Zn-impregnated samples, UV-Vis spectra in Figure 13 shows a distinctive band gap absorption at 27 000 cm^{-1}, this is typical for the presence of ZnO in the sample.[53] Besides the ZnO band gap absorption, no significant changes due to impregnation with Zn are seen as the Cu^{2+} d-d transitions and peaks at 41 800 cm^{-1} and 45 000 cm^{-1} remain at same location i.e. Cu^{2+} and copper oxide species remain unchanged. Formation of the ZnO seen in the UV-Vis, is in agreement with the XRD pattern for the same sample (in Figure 9), as discussed earlier.

The results from N_2 physisorption measurements are presented in the Table 1. In the table, values from the study by Sommer *et al.* for H-SSZ-13 (Si:Al 14) are reproduced for a reference,[38] while rest of the values are presented as received from the results obtained for samples sent to an external laboratory for the N_2 physisorption measurements. In the table, external surface area refers to sum of external surface of the crystal and the surfaces on the pores which are larger than micropores.

From values for the steamed and impregnated samples in the Table 1 it becomes apparent that the performed steaming procedure has not been reproduced in a decent manner. As described in the experimental section, two batches of Cu-SSZ-13 with different sample sizes (3 133 mg and 3 615 mg) were steamed at 730 °C. The sample from steamed batch with mass 3 133 mg was used as the steamed reference and another sample from same batch was impregnated with Pt. From the batch of 3 615 mg, samples impregnated with Ca, P and Zn were prepared. As can be seen in the Table 1, all of the samples impregnated with Ca, P or Zn express significantly larger BET and micropore surface areas and micropore volumes than the steamed reference sample. This should not be possible as commonly the mentioned values decrease upon impregnation as the catalyst pores are blocked, preventing the N_2 molecules from diffusing to the pores. The most likely explanation is the most obvious one; the two differently sized steaming batches resulted in grossly different parent materials for the impregnations. The effect of the different parent materials will be clearly seen in the following section, where catalytic tests are discussed.

As the suggested earlier by the XRD, UV-Vis and IR results, the steaming treatment results in degradation of the SSZ-13 framework and the same crystal structure degradation is evident from the N_2 physisorption results in Table 1. As compared to the reference calcined H-SSZ-13 BET and micropore surface areas and micropore volume, all steam treated Cu-SSZ-13 samples (with or without impregnation) exhibit vastly smaller values which might indicate partial destruction of the

SSZ-13 framework due to degraded framework structure.[38] On the other hand, for the only steamed Cu-SSZ-13 the external surface area is seen to increase from 25 m^2/g to 36 m^2/g, as compared to the H-SSZ-13 reference, a phenomena which has been assigned to mesopore formation to the framework structure due to degradation of the framework.[38] For the Pt impregnated sample, the measured micropore surface area and micropore volume drop which is indicative to micropore blocking caused by formation of Pt^0 species seen in the XRD results earlier. As the external surface area remains unchanged, the supposedly formed mesopores do not seem to be affected by the impregnation with Pt.

For rest of the steamed and subsequently impregnated samples (Ca, P and Zn), no parent steamed only Cu-SSZ-13 sample were sent for the N_2 physisorption measurements and the effect of impregnation on the accessible catalyst surfaces cannot be unambiguously assessed. However, within the impregnated Ca, P or Zn impregnated samples, the order of micropore surface areas is Zn>P>Ca, Zn having highest measured micropore surface area of 373 m^2/g, P having micropore surface of 353 m^2/g and Ca having the lowest value of 332 m^2/g. For the P impregnated sample, the

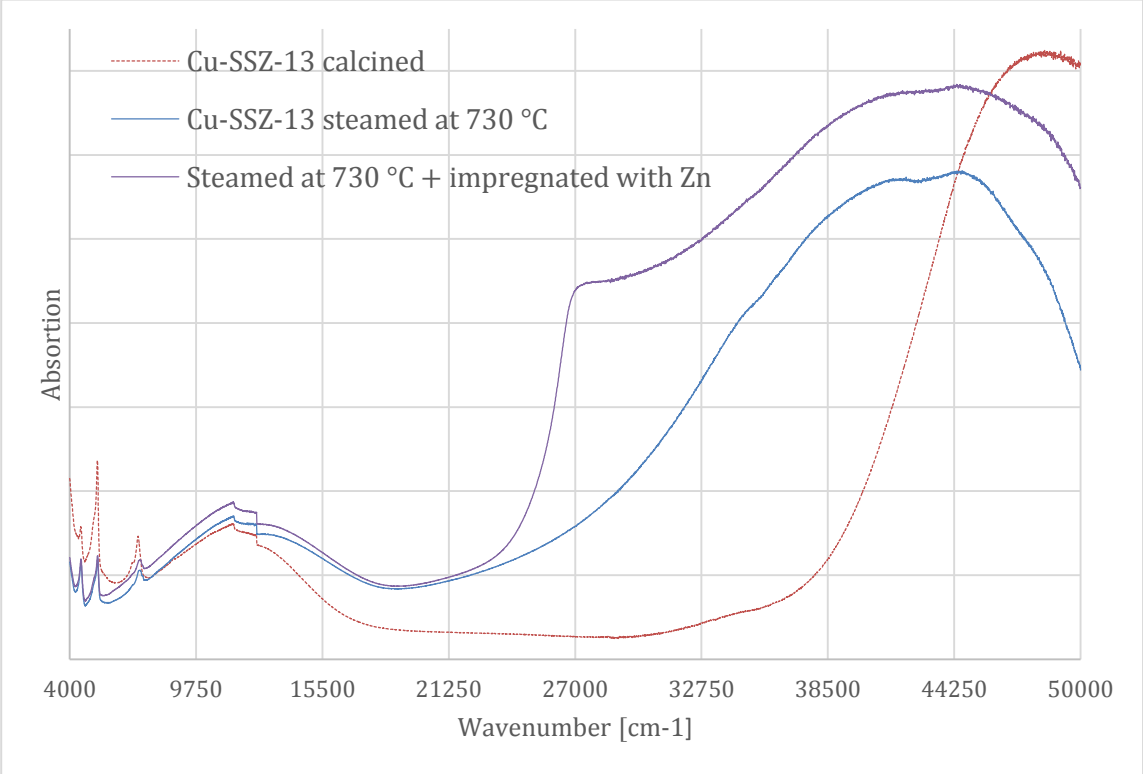

Figure 13: The UV-Vis spectra of calcined Cu-SSZ-13 sample, Cu-SSZ-13 sample steamed at 730 °C for 13h and Cu-SSZ-13 which has been steamed at 730 °C for 13h and then impregnated with Zn.

external surface area decreases most which might indicate that also the mesopores possibly formed due to steaming might also be somewhat more blocked with P than with Ca and Zn species.

Table 1: The N_2 physisorption results received from the external laboratory and reported as received. Values for H-SSZ-13 reproduced from reference 38 for comparison. Micropore and external surface areas and micropore volume obtained with the t-plot method.

	BET surface (the total surface area) [m^2/g]	Micropore surface [m^2/g]	External surface [m^2/g]	Micropore volume [cm^3/g]
H-SSZ-13(1	704	679	25	0.25
Cu-SSZ-13 steamed at 730 ˚C(2	323	288	36	0.11
Cu-SSZ-13 steamed at 730 ˚C + Pt impregnated(2	310	273	36	0.10
Cu-SSZ-13 steamed at 730 ˚C + Ca impregnated(3	357	332	25	0.13
Cu-SSZ-13 steamed at 730 ˚C + P impregnated(3	373	353	21	0.13
Cu-SSZ-13 steamed at 730 ˚C + Zn impregnated(3	402	373	28	0.14

1) Values from reference 38 (Si:Al ratio 14)
2) Samples from same parent (steamed sample 3 133 mg)
3) Samples from same parent (steamed sample 3 615 mg)

3.4 NH_3-SCR catalytic testing

The catalytic testing in the NH_3-SCR reaction for Cu-SSZ-13 samples steamed at 730 °C and subsequently impregnated with Ca, P, Pt or Zn as the deactivating species, was performed with the set up schematically drawn in the Figure 5 and discussed in section 2.4. Input gas values were 896 ppm for NO and 945 NH_3 ppm for NH_3 to simulate the Standard SCR reaction (1). Steady-state was assumed and the same GHSV of 67 500 h^{-1} was used for all the catalytic tests, as introduced earlier in section 2.4. All gas output values reported in the study for the catalytic tests were obtained from measurements with the $DeNO_x$ IR, as the measured MS values were found to be highly dependent on the used calibration and gave absolute values which deviated strongly from the results obtained with the $DeNO_x$ IR. Therefore, as $DeNO_x$ data was deemed to be more reliable in these particular measurements and was used to calculate the output gas concentrations. As N_2 is IR inactive and its output concentration cannot be determined by using only the $DeNO_x$ IR, discussion regarding the selectivity of the NO conversions is done with measured output gas concentrations of NO, N_2O and NO_2 (as ppm) and are presented in the Table 2 with the corresponding NO conversions. The Cu-

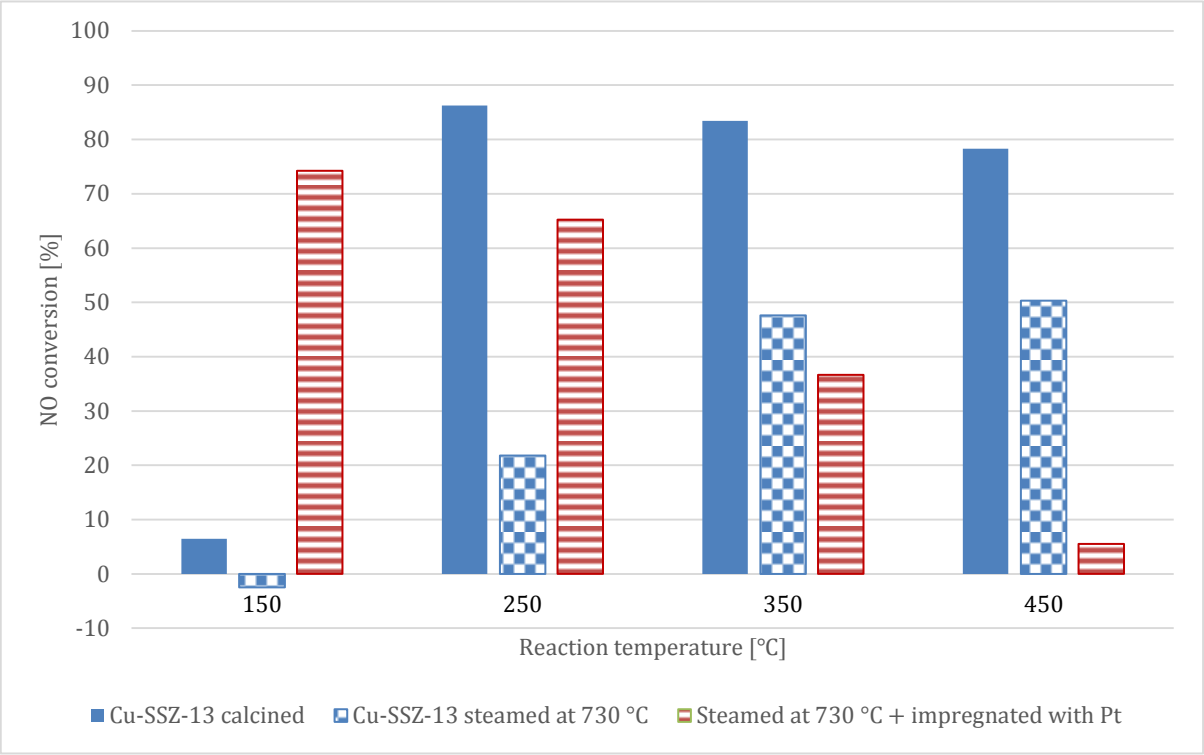

Figure 14: NO conversions measured under the Standard SCR reaction for calcined Cu-SSZ-13, Cu-SSZ-13 sample steamed at 730 °C for 13h and for Cu-SSZ-13 steamed at 730 °C for 13h and then impregnated with Pt. Both, only steamed and steamed and subsequently Pt impregnated sample originate from the same parent. For all measurements GHSV of 67 500 h^{-1} was used.

SSZ-13 catalyst has been previously deemed stable under similar reaction conditions for NH_3-SCR as used in the present study,[12] and catalyst stability is not discussed here.

As discussed in the end of previous section 3.3, the N_2 physisorption data in Table 1 shows that the parent samples which were steamed at 730 °C and subsequently used for impregnation were not identical. For the catalytic tests, Cu-SSZ-13 sample steamed at 730 °C and the sample subsequently impregnated with Pt originated from same the parent (from the steamed batch of 3 133 mg). Rest of the samples steamed and impregnated, with either Ca, P or Zn, were prepared from the different parent (from the steamed batch of 3 615 mg). These samples prepared from the different parents for the catalytic tests are unfortunately not comparable as the N_2 physisorption results revealed that the two different steamed Cu-SSZ-13 batches were grossly different (see Table 1 and the discussion in the previous section regarding the N_2 physisorption results). Therefore, in the Figure 14 are presented the comparable results from same parent and in the Figure 15 are presented the catalytic test results for the samples originating from the other parent. The same

calcined only Cu-SSZ-13 sample was used as reference for both of the sample sets, which originates from a yet another parent.

First of all regarding catalytic testing results, strong deactivation effect of the steaming treatment at 730 °C can be seen in the Figure 14. Upon applied steam treatment at 730 °C, the catalytic activity of the Cu-SSZ-13 catalyst drops over every measured reaction temperature. At 150 °C, no NO conversion usually takes place as the H_20 might compete for the adsorption sites on the catalyst, inhibiting the reaction,[7,17,60] and might at least partly explain the low NO conversions at the temperature of 150 °C for the NH_3-SCR (with the exception of the Pt-impregnated sample, which will be discussed later). As the reaction temperature rises from 250 °C to 450 °C, the steamed Cu-SSZ-13 regains its NO conversion ability somewhat. In general, this seems to be a trend for zeolite catalysts in NH_3-SCR, i.e. hydrothermal treatment has more detrimental effect on the low reaction temperatures than on high temperatures.[3–5,34] For the steamed sample tested here, best explanation for the lost activity is most likely to be due to the loss of catalytically active Cu^{2+} sites resulting from the degrading SSZ-13 framework. As seen and discussed in the XRD, UV-Vis, IR and N_2 physisorption results prior, due to steaming treatment the Cu-SSZ-13 framework structure degrades causing lost catalyst surface area and formation of copper oxides, which are deemed catalytically inactive for the NH_3-SCR reaction.[43] Why the steamed samples lose relatively more activity at lower temperatures, cannot be explained here with the available results.

Besides the lost activity, upon steaming the calcined Cu-SSZ-13, from Table 2 it can be seen that the steaming treatment caused progressively increasing formation of N_2O from 1 to 24 ppm as the reaction temperature was increased from 150 °C to 450 °C. Over the same temperature range, NO_2 formation is within 1-8 ppm. For calcined only Cu-SSZ-13 sample, as the reaction temperature increases over the same range, the NO_2 side-product formation increases from 6 to 43 ppm while N_2O formation stays within range 1-5 ppm. As a conclusion, upon steaming the Cu-SSZ-13 sample the formed side-product composition changes from NO_2 towards formation of N_2O. Change in the side-product composition, suggests that some new species might have been formed due to steaming treatment which possesses mild catalytic properties or possibly the reaction pathways and their relative importance may have changed. Possible candidates, as according the characterizations discussed prior, for the mildly catalytically active species could be the likely formed copper oxides, species formed from the Al removed from the framework locations or formed defect sites at the SSZ-13 framework structure.

A catalytically active species due to impregnation performed was formed upon the introduction of the Pt species on the Cu-SSZ-13 catalyst. As was discussed earlier, from the XRD patterns it can be seen that metallic Pt^0 was formed upon impregnation, species which is known to be very active catalyst towards oxidation reactions.[19] Indeed, catalytic activity of the formed Pt^0 can be observed in the performed catalytic tests in the Figure 14.

Already at low temperature of 150 °C, the Pt-impregnated catalyst shows very high activity. As noted earlier, at 150 °C the NH_3-SCR reaction is not very active which might be due to competing absorption by the H_2O.[7,17,60] However, when the steamed Cu-SSZ-13 sample is impregnated with the Pt, the catalyst shows already high activity from on 150 °C i.e. probably another reaction than the NH_3-SCR has become dominant. It might seem from the Figure 14 that the catalytic activity of the steamed and Pt-impregnated Cu-SSZ-13 catalyst drops upon increasing the reaction temperature but this assumption can be deemed to be false when the N_2O and NO_2 formations from Table 2 are taken into consideration for the catalytic test for the Pt-impregnated sample. As the reaction temperature increases, the output gases shift from production of N_2O at low temperatures to majority output of NO_2 and NO at higher temperatures, i.e. the ratio of the output gases changes from N_2O preference towards preferred formation of NO_2 and NO. Not shown here, but from the $DeNO_x$ IR gas profile for the experiment, virtually no NH_3 was seen in the output gas feed i.e. most likely it served as a source for oxidation reaction as catalysed by the formed Pt^0. According the N_2 physisorption data in the Table 1, some catalyst pore blocking is introduced upon impregnation with Pt as the micropore surface and volume are both decreased. This supports the idea of formation of catalytically active species upon the impregnation as otherwise the catalyst activity should only drop as the catalytically active sites in the steamed Cu-SSZ-13 are blocked.

Also, formation of NH_4NO_3 was observed for the Pt impregnated catalyst as it adsorpted on the unheated $DeNO_x$ IR cell giving absorption peaks assignable to the NH_4NO_3 species (see the $DeNO_x$ IR spectrum in Appendix Figure B-5),[61] of which formation is known to occur in NH_3-SCR.[14] Therefore, taking the above mentioned matters into consideration, impregnating steamed Cu-SSZ-13 with Pt caused formation of active yet unselective catalyst as side-products N_2O and/or NO_2 are formed in high amounts over the whole measured temperature range and at least some undesired NH_4NO_3 is also created.

Catalytic test results of the samples steamed at 730 °C and subsequently impregnated with Ca, P or Zn, which originate from the same steamed parent material, are presented Figure 15. As no steamed only sample from the same parent material was tested for the NH_3-SCR, no comparison

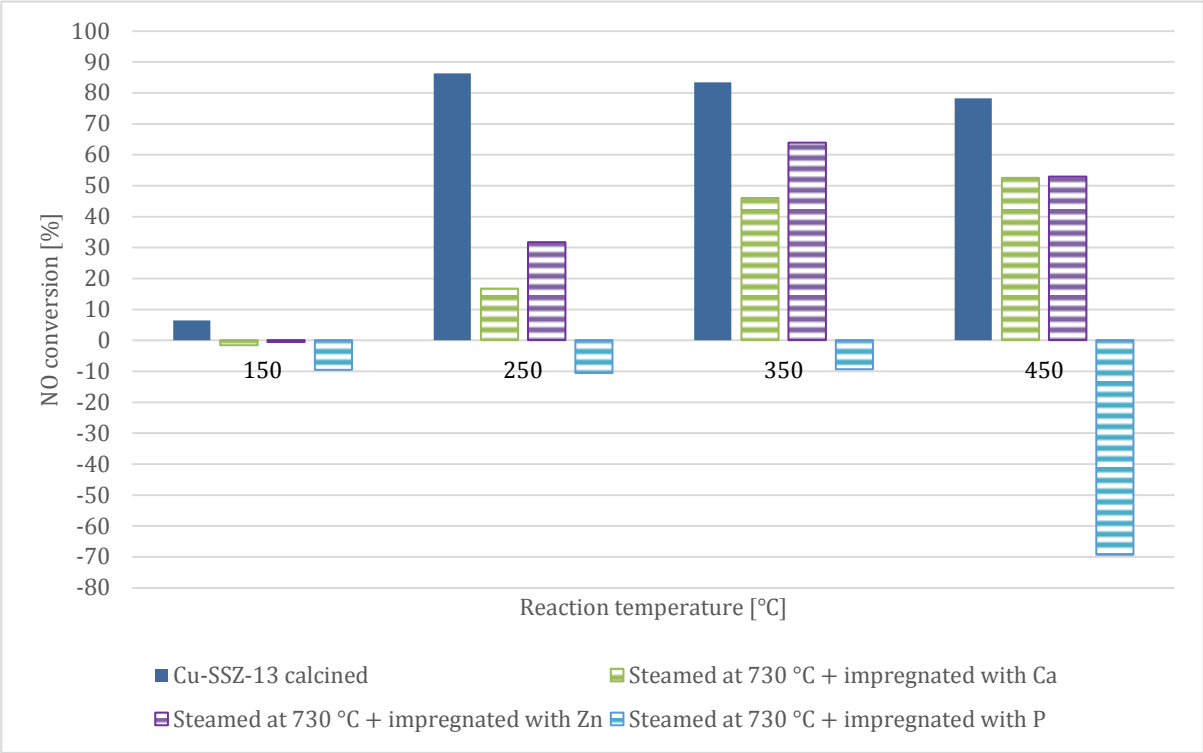

Figure 15: NO conversions measured under the Standard SCR reaction for calcined Cu-SSZ-13, Cu-SSZ-13 sample steamed at 730 °C for 13h and for Cu-SSZ-13 steamed at 730 °C for 13h and then subsequently impregnated with Ca, P or Zn. Each, only steamed and steamed and subsequently Ca, P or Zn impregnated samples originate from same parent. For all measurements GHSV of 67 500 h^{-1} was used.

between the effect of steaming only and additional impregnation could be done. In the following, therefore, only the relative effects of the impregnated species to each other are discussed. For these samples also, results from catalytic test for the same calcined Cu-SSZ-13 as previously, was used as the reference.

As comparing the impregnated samples of steamed Cu-SSZ-13, the most severe loss in the total catalyst surface area is due to Ca with BET of 357 m^2/g, which is followed by P with BET of 373 m^2/g while the Zn has the least effect on the total surface area, with measured BET of 402 m^2/g. The NO conversion results for the samples, in the Figure 15 shows a trend which deviates from these BET values a bit. The worst catalyst deactivation is due to impregnation with P which causes complete inactivity towards the NO conversion to N_2 over all the measured reaction temperatures. Second worst catalyst deactivator is the impregnation with Ca and the least deactivating of the three species used is the Zn. As the catalyst deactivation due to impregnation does not directly

follow the same trend as the lost total surface of the catalyst, more deactivating effects might be present than just diffusion limitations due to pore blocking and restricted access to the active sites.

Impregnating the steamed Cu-SSZ-13 with P has a very detrimental effect on the catalyst activity over all the measured reaction temperatures, as can be seen from the Figure 15. Upon impregnating the Cu-SSZ-13 with P, the catalyst is completely deactivated over the temperature range of 150 - 350 °C as steady negative conversions can be interpreted as the input NO flowing through the catalyst and the reactor tube unreacted. Negative conversions are most likely due to measurement error with the $DeNO_x$ IR, which seems to systematically overestimate the amount of NO in the output stream, leading to negative conversions through equation (4). The most likely cause for the overestimated NO output values could be a too large adsorption coefficient used for the conversion of the NO absorptions from the $DeNO_x$ IR spectrum to the absolute NO output gas concentrations through the Beer-Lambert law. At 450 °C, the NO conversion grows significantly negative marking noticeable increase in the NO output i.e. the catalyst is actually producing more NO instead of removing it from the stream. The source for the NO formation needs to be the other input gas, i.e. NH_3, present in the gas input feed. This indeed can be seen from the $DeNO_x$ IR gas profile (in Appendix, Figure B-6) of the experiment for the P impregnated sample as the NH_3 is consumed at the reaction temperature of 450 °C while NO output increases.

As an unexpected effect, seems like the P impregnation might have formed a new catalytically active species which seems to oxidize NH_3 to NO in an unknown reaction at the reaction temperature of 450 °C. As from the literature, more commonly the P impregnation has an effect of deactivating the zeolite catalyst due to diffusion limitations,[9,26] but no catalytically active P species have been observed for the NH_3-SCR. Referring to the discussion earlier in the UV-Vis result section for the P-impregnated sample, if a P species is formed, it might be a copper phosphate. However, no precise reaction for any type of copper phosphate activity towards NH_3 oxidation could immediately be found. Also, from Table 2 it can be seen that at 450 °C the P-impregnated sample produces more of both, the N_2O and NO_2 as compared to the steamed only Cu-SSZ-13 sample. This could also be taken as another indication that catalytically active species could have formed as a consequence of the impregnation with P. To sum up the effect of P impregnation, over the reaction temperature range of 150-350 °C the catalyst is completely deactivated due to diffusion limitations while at 450 °C some unknown species seems to oxidate NH_3 to NO in an unknown reaction.

The catalytic testing with Ca- and Zn-impregnated samples let to results resembling each other, as presented in the Figure 15. At 150 °C, no NO or very little NO conversion takes place. At 250 °C

and 350 °C, NO conversions are regained somewhat and with Zn to somewhat higher degree as compared to the Ca-impregnated sample. At 450 °C, both Ca- and Zn-impregnated catalyst have near identical NO conversions. The trends seem to seem to follow the micropore surface areas in the Table 1, for the more deactivated Ca-impregnated sample the micropore surface area is lower than for the less deactivated Zn-impregnated sample. As the catalyst micropore surface area is smaller, less catalyst surface area (i.e. active sites) is available as the micropores on the catalyst are blocked by the impregnation species, resulting in lower NO conversion. That is, for Ca and Zn impregnations the catalyst deactivation seems to be due to diffusion problems caused by micropore blocking preventing the reactants to reach active sites inside the zeolite pores. Why the NO conversions is identical for both at 450 °C even though the BET surfaces are vastly different, is a hard question to answer with available information and further investigations are needed. However, as looking to the Table 2 for N_2O and NO_2 side-product formation for Ca and Zn-impregnated samples, Zn produces somewhat higher amounts of N_2O in overall, and at 450 °C, Zn-impregnated catalyst causes NO_2 formation of 40 ppm while Ca-impregnated catalyst forms only 6 ppm of NO_2 at the same reaction temperature. In total, impregnating the steamed Cu-SSZ-13 with Ca lowers the NO conversion activity to higher degree than impregnation with Zn while impregnation with Zn causes higher loss in reaction selectivity than impregnation with Ca.

For the Zn-impregnated samples, from XRD and UV-Vis, ZnO was found to form upon impregnation and is the most likely cause for the lost micropore surface due to pore blocking of the micropores in the catalyst. Similar results were found by Kern *et al.* who have impregnated their non-hydrothermally treated Fe-MFI with $Zn(NO_3)_2$ and observed catalyst deactivation in NH_3-SCR even for low amounts of impregnated Zn. Deactivation effect was assigned to the diffusion limitations due to formed ZnO.[26] Furthermore, in a review article by Hamada, ZnO was mentioned as somewhat catalytically active species for HC-SCR as starting from reaction temperature of 450 °C.[62] If the ZnO is also catalytically active for the observed formation of NO_2 at 450 °C in the present case, it would needed to be investigated with further studies for confirmation.

For the Zn impregnation the cause of catalyst deactivation seems to be rather clearly due to ZnO but for Ca impregnation, the catalyst deactivating species cannot be unambigously determined within this study. Most commonly, CaO is deemed to cause pore blocking on zeolite catalyst and therefore decreased catalyst activity in NH_3-SCR.[26] No formation of CaO is seen in the present study but such species might still be present and explain the lost micropore surface area. According to UV-Vis results for Ca impregnation in Figure 12, at least some Ca^{2+} could be present on the impregnated catalyst. But whether Ca^{2+} ions could solely cause the pore blocking or whether the

Ca^{2+} ions are just a minor fraction of the total Ca species present and therefore playing an insignificant role on the catalyst deactivation, cannot be answered within this study. Whatever the Ca species causing the pore blocking might be, it does not seem to have any significant catalytic properties as the changes in side-product, N_2O and NO_2 (Table 1), formations due to Ca impregnation are rather low.

Table 2: NO conversions and output ppm values for N_2O, NO and NO_2 as measured from the output gas feed with DeNOx IR. All measurements were done under the Standard SCR reaction with GHSV of 67 500 h^{-1} with assumption of steady-state.

Catalyst	Reaction temperature [°C]	NO conversion [%]	Output [ppm] N2O	NO	NO2
Cu-SSZ-13 calcined	150	6	1	838	6
	250	86	3	123	1
	350	83	5	148	7
	450	78	3	195	43
Cu-SSZ-13 steamed at 730 °C	150	-2	1	918	4
	250	22	12	701	4
	350	48	16	470	1
	450	50	24	445	8
Steamed at 730 °C + impregnated with Ca	150	-2	1	910	5
	250	17	8	747	6
	350	46	16	484	1
	450	52	19	426	6
Steamed at 730 °C + impregnated with P	150	-10	3	982	8
	250	-11	3	991	8
	350	-9	14	980	1
	450	-69	30	1518	12
Steamed at 730 °C + impregnated with Pt	150	74	595	231	2
	250	65	540	312	66
	350	37	269	568	299
	450	6	79	847	396
Steamed at 730 °C + impregnated with Zn	150	-1	2	901	4
	250	32	19	612	2
	350	64	20	324	0
	450	53	23	422	40

4 CONCLUSIONS AND FUTURE OUTLOOK

Several conclusions can be drawn from the performed characterizations and catalytic tests under the Standard SCR conditions in the NH_3-SCR reaction, as regarding the deactivation of the steamed only and steamed and subsequently Ca, P, Pt or Zn impregnated Cu-SSZ-13 samples.

Steaming the Cu-SSZ-13 sample at 730 °C for 13h causes substantial loss in the catalytic activity in the NH_3-SCR reaction which is due to degradation of the framework structure by the dealumination process as the Al is removed from the framework. Upon the removal of the framework Al, the catalytically active Cu^{2+}-ions are subject to sintering, forming catalytically inactive copper oxides and therefore decreasing the amount of active sites for NH_3-SCR which is seen as lost NO conversion over the whole measured temperature range of 150 – 450 °C.

For resolving the effect of deactivating chemical species Ca, P, Pt and Zn, on the hydrothermally treated catalyst, Cu-SSZ-13 samples were first steamed at 730 °C and then subsequently impregnated with either Ca, P, Pt or Zn via Wet Impregnation. The two different steamed parent Cu-SSZ-13 samples used for the impregnations were found to be grossly different by the N_2 physisorption measurements and therefore, catalytic tests were found not to be easily comparable.

Impregnation of the steamed catalyst with Pt lead to formation of highly oxidizing Pt^0 species on the catalyst which caused the Pt-impregnated catalyst to become highly active yet completely unselective towards formation of N_2 over all of the measured reaction temperatures from 150 °C to 450 °C as high amounts of N_2O or NO_2 were formed.

Impregnation of the steamed Cu-SSZ-13 with P caused complete loss of catalytic activity over the reaction temperature range of 150 - 350 °C, deactivation which is most likely due to diffusion limitations introduced upon the P impregnation. At reaction temperature of 450 °C NH_3 is seen to oxidize to NO, increasing the NO output to a higher level than in the input feed. From the characterization results it might be suspected that a catalytically active copper phosphate species may have formed upon impregnation with P, however, no conclusive evidence could be presented.

Ca impregnation of the steamed Cu-SSZ-13 had somewhat more deactivating effect than the Zn impregnation on the reaction temperatures of 250 °C and 350 °C in the NH_3-SCR. At 450 °C, both Ca and Zn impregnated samples exhibited same NO conversion activity although Zn impregnated sample with somewhat poorer selectivity as NO_2 was formed as a side-product. For both, the deactivation seems to be due to diffusion limitations, as especially for Ca, the accessible catalyst

surface dropped significantly. For the Zn, diffusion limitations are most likely due to formed ZnO while for Ca the diffusion limiting species remains uncertain as only Ca^{2+} was observed.

Therefore, to conclude; P and Pt species are severe deactivating species for the NH_3-SCR under hydrothermal reaction conditions and Ca shows more deactivating effect that the Zn.

The results obtained here could be used as a base for further studies on the topic. Most notably, several topics observed could be interesting to investigate further;

i. The identity and confirm the presence of the possible copper phosphate species.
ii. The species formed due to Ca impregnation
iii. The origins of the higher deactivation of the catalyst due to steaming treatment over low reaction temperatures as compared to high reaction temperatures.

Besides the above mentioned topics, the catalytic testing for the Ca, P, Pt and Zn species should be repeated with identical parent, for decent comparison of the catalytic test results and the deactivating effects. Also, the used steaming method could be investigated a bit further to gain knowledge under which conditions identical hydrothermal treatment is achieved.

In addition to the mentioned topics, to further develop the knowledge about deactivation phenomena in the real life NH_3-SCR systems with Cu-SSZ-13 catalyst, studies would be needed where all the deactivating chemical species are introduced on the catalyst at the same time, as opposite to the separate introduction done here. And also, the deactivation chemical species should be introduced in the gas phase and at the same time as the NH_3-SCR gas input feed, which would represent the real operation conditions of the NH_3-SCR system with some added accuracy. Then, whether the laboratory based experiments correspond the actual catalyst deactivating phenomena in the real system could perhaps be assessed more carefully.

A BIBLIOGRAPHY

1. Brandenberger, S.; Krocher, O.; Tissler, A.; Althoff, R. The State of the Art in Selective Catalytic Reduction of NOx by Ammonia Using Metal-Exchanged Zeolite Catalysts. *Catalysis Reviews - Science and Engineering* **2008**, *50*, 492–531.

2. Kwak, J. H.; Tonkyn, R. G.; Kim, D. H.; Szanyi, J.; Peden, C. H. F. Excellent Activity and Selectivity of Cu-SSZ-13 in the Selective Catalytic Reduction of NOx with NH3. *Journal of Catalysis* **2010**, *275*, 187–190.

3. Kwak, J. H.; Tran, D.; Burton, S. D.; Szanyi, J.; Lee, J. H.; Peden, C. H. F. Effects of Hydrothermal Aging on NH3-SCR Reaction over Cu/zeolites. *Journal of Catalysis* **2012**, *287*, 203–209.

4. Ye, Q.; Wang, L.; Yang, R. T. Activity, Propene Poisoning Resistance and Hydrothermal Stability of Copper Exchanged Chabazite-like Zeolite Catalysts for SCR of NO with Ammonia in Comparison to Cu/ZSM-5. *Applied Catalysis, A: General* **2012**, *427-428*, 24–34.

5. Fickel, D. W.; D'Addio, E.; Lauterbach, J. A.; Lobo, R. F. The Ammonia Selective Catalytic Reduction Activity of Copper-exchanged Small-pore Zeolites. *Applied Catalysis, B: Environmental* **2011**, *102*, 441–448.

6. Schmieg, S. J.; Oh, S. H.; Kim, C. H.; Brown, D. B.; Lee, J. H.; Peden, C. H. F.; Kim, D. H. Thermal Durability of Cu-CHA NH3-SCR Catalysts for Diesel NOx Reduction. *Catalysis Today* **2012**, *184*, 252–261.

7. Metkar, P. S.; Balakotaiah, V.; Harold, M. P. Experimental and Kinetic Modeling Study of NO Oxidation: Comparison of Fe and Cu-zeolite Catalysts. *Catalysis Today* **2012**, *184*, 115–128.

8. Gosta-Sjoberg, S. Vanadium Pentoxide Dust: a Clinical and Experimental Investigation on Its Effect after Inhalation. *British Journal of Industrial Medicine* **1950**, *7*, 195–196.

9. W. E. J., K. van; Krijnsen, H. C.; C. M., den B. van; Calis, H. P. A. Deactivation of Zeolite Catalysts Used for NOx Removal. *Applied Catalysis, B: Environmental* **2000**, *25*, 125–135.

10. Rokosz, M. J.; Chen, A. E.; Lowe-Ma, C. K.; Kucherov, A. V; Benson, D.; Paputa M. C., P.; McCabe, R. W. Characterization of Phosphorus-poisoned Automotive Exhaust Catalysts. *Applied Catalysis, B: Environmental* **2001**, *33*, 205–215.

11. Krocher, O.; Elsener, M. Chemical Deactivation of V2O5/WO3-TiO2 SCR Catalysts by Additives and Impurities from Fuels, Lubrication Oils, and Urea Solution. *Applied Catalysis, B: Environmental* **2008**, *77*, 215–227.

12. Korhonen, S. T.; Fickel, D. W.; Lobo, R. F.; Weckhuysen, B. M.; Beale, A. M. Isolated Cu2+ Ions: Active Sites for Selective Catalytic Reduction of NO. *Chemical communications (Cambridge, England)* **2011**, *47*, 800–802.

A BIBLIOGRAPHY

13. Kwak, J. H.; Tran, D.; Szanyi, J.; Peden, C. H. F.; Lee, J. H. The Effect of Copper Loading on the Selective Catalytic Reduction of Nitric Oxide by Ammonia Over Cu-SSZ-13. *Catalysis Letters* **2012**, *142*, 295–301.

14. Metkar, P. S.; Balakotaiah, V.; Harold, M. P. Experimental Study of Mass Transfer Limitations in Fe- and Cu-zeolite-based NH3-SCR Monolithic Catalysts. *Chemical Engineering Science* **2011**, *66*, 5192–5203.

15. Deka, U.; Juhin, A.; Eilertsen, E. A.; Emerich, H.; Green, M. A.; Korhonen, S. T.; Weckhuysen, B. M.; Beale, A. M. Confirmation of Isolated Cu2+ Ions in SSZ-13 Zeolite as Active Sites in NH3-Selective Catalytic Reduction. *Journal of Physical Chemistry C* **2012**, *116*, 4809–4818.

16. Yang, X.; Wu, Z.; Moses-Debusk, M.; Mullins, D. R.; Mahurin, S. M.; Geiger, R. A.; Kidder, M.; Narula, C. K. Heterometal Incorporation in Metal-Exchanged Zeolites Enables Low-Temperature Catalytic Activity of NOx Reduction. *Journal of Physical Chemistry C* **2012**, *116*, 23322–23331.

17. Zhu, H.; Kwak, J. H.; Peden, C. H. F.; Szanyi, J. In Situ DRIFTS-MS Studies on the Oxidation of Adsorbed NH3 by NOx over a Cu-SSZ-13 Zeolite. *Catalysis Today* **2013**, *205*, 16–23.

18. Bartholomew, C. H. Mechanisms of Catalyst Deactivation. *Applied Catalysis, A: General* **2001**, *212*, 17–60.

19. Regalbuto, J. *Catalyst Preparation: Science and Engineering*; Regalbuto, J., Ed.; 1st ed.; CRC Press, 2007.

20. Masuda, T.; Fujikata, Y.; Mukai, S. R.; Hashimoto, K. Changes in Catalytic Activity of MFI-type Zeolites Caused by Dealumination in a Steam Atmosphere. *Applied Catalysis, A: General* **1998**, *172*, 73–83.

21. Sokol, A. A.; Catlow, C. R. A.; Garces, J. M.; Kuperman, A. Local States in Microporous Silica and Aluminum Silicate Materials. 1. Modeling Structure, Formation, and Transformation of Common Hydrogen Containing Defects. *Journal of Physical Chemistry B* **2002**, *106*, 6163–6177.

22. Bhering, D. L.; Ramirez-Solis, A.; Mota, C. J. A. A Density Functional Theory Based Approach to Extraframework Aluminum Species in Zeolites. *Journal of Physical Chemistry B* **2003**, *107*, 4342–4347.

23. Isernia, L. F. FTIR Study of the Relation, Between Extra-framework Aluminum Species and the Adsorbed Molecular Water, and Its Effect on the Acidity in ZSM-5 Steamed Zeolite . *Materials Research* **2013**, *16* , 792–802.

24. Kawai, T.; Tsutsumi, K. A Study on the Surface Silanol Groups Developed by Hydrothermal and Acid Treatment of Faujasite Type Zeolites. *Journal of Colloid and Interface Science* **1999**, *212*, 310–316.

25. Angove, D. E.; Cant, N. W. Position Dependent Phenomena During Deactivation of Three-way Catalytic Converters on Vehicles. *Catalysis Today* **2000**, *63*, 371–378.

26. Kern, P.; Klimczak, M.; Heinzelmann, T.; Lucas, M.; Claus, P. High-throughput Study of the Effects of Inorganic Additives and Poisons on NH3-SCR Catalysts. Part II: Fe-zeolite Catalysts. *Applied Catalysis, B: Environmental* **2010**, *95*, 48–56.

27. Yan, J. Y.; Lei, G.-D.; Sachtler, W. M. H.; King, H. H. Deactivation of Cu/ZSM-5 Catalysts for Lean NOx Reduction: Characterization of Changes of Cu State and Zeolite Support. *Journal of Catalysis* **1996**, *161*, 43–54.

28. Weitkamp, J. Zeolites and Catalysis. *Solid State Ionics* **2000**, *131*, 175–188.

29. Deka, U.; Lezcano-Gonzalez, I.; Warrender, S. J.; Lorena A., P.; Wright, P. A.; Weckhuysen, B. M.; Beale, A. M. Changing Active Sites in Cu-CHA Catalysts: deNOx Selectivity as a Function of the Preparation Method. *Microporous and Mesoporous Materials* **2013**, *166*, 144–152.

30. Goltl, F.; Bulo, R. E.; Hafner, J.; Sautet, P. What Makes Copper-Exchanged SSZ-13 Zeolite Efficient at Cleaning Car Exhaust Gases?. *Journal of Physical Chemistry Letters* **2013**, *4*, 2244–2249.

31. Deka, U.; Lezcano-Gonzalez, I.; Weckhuysen, B. M.; Beale, A. M. Local Environment and Nature of Cu Active Sites in Zeolite-Based Catalysts for the Selective Catalytic Reduction of NOx. *ACS Catalysis* **2013**, *3*, 413–427.

32. Schoonheydt, R. A. UV-vis-NIR Spectroscopy and Microscopy of Heterogeneous Catalysts. *Chemical Society Reviews* **2010**, *39*, 5051–5066.

33. Diaz-Cabanas, M.-J.; Barrett, P. A. Synthesis and Structure of Pure SiO2 Chabazite: The SiO2 Polymorph with the Lowest Framework Density. *Chemical Communications (Cambridge)* **1998**, 1881–1882.

34. Moliner, M.; Franch, C.; Palomares, E.; Grill, M.; Corma, A. Cu-SSZ-39, an Active and Hydrothermally Stable Catalyst for the Selective Catalytic Reduction of NOx. *Chemical Communications (Cambridge, United Kingdom)* **2012**, *48*, 8264–8266.

35. Stuart, B. *Infrared Spectroscopy: Fundamentals and Applications*; John Wiley & Sons, Ltd, 2004.

36. Karge, H. G. Characterization of Zeolites by Infrared Spectroscopy. *Microporous and Mesoporous Materials* **1998**, *22*, 547–549.

37. Barbera, K.; Bonino, F.; Bordiga, S.; Janssens, T. V. W.; Beato, P. Structure-deactivation Relationship for ZSM-5 Catalysts Governed by Framework Defects. *Journal of Catalysis* **2011**, *280*, 196–205.

38. Sommer, L.; Mores, D.; Svelle, S.; Stoecker, M.; Weckhuysen, B. M.; Olsbye, U. Mesopore Formation in Zeolite H-SSZ-13 by Desilication with NaOH. *Microporous and Mesoporous Materials* **2010**, *132*, 384–394.

39. Smith, J. V; Knowles, C. R.; Rinaldi, F. Crystal Structures with a Chabazite Framework. III. Hydrated Ca Chabazite at +20 and -150°. *Acta. Cryst.* **1964**, *17*, 374–383.

40. Ren, L.; Zhang, Y.; Zeng, S.; Zhu, L.; Sun, Q.; Zhang, H.; Yang, C.; Meng, X.; Yang, X.; Xiao, F.-S. Design and Synthesis of a Catalytically Active Cu-SSZ-13 Zeolite from a Copper-amine Complex Template. *Cuihua Xuebao* **2012**, *33*, 92–105.

41. Groothaert, M. H.; Jeroen A., B. Van; Battiston, A. A.; Weckhuysen, B. M.; Schoonheydt, R. A. Bis(μ-oxo)dicopper in Cu-ZSM-5 and Its Role in the Decomposition of NO: A Combined in Situ XAFS, UV-Vis-Near-IR, and Kinetic Study. *Journal of the American Chemical Society* **2003**, *125*, 7629–7640.

42. Praliaud, H.; Mikhailenko, S.; Chajar, Z.; Primet, M. Surface and Bulk Properties of Cu-ZSM-5 and Cu/Al2O3 Solids During Redox Treatments. Correlation with the Selective Reduction of Nitric Oxide by Hydrocarbons. *Applied Catalysis, B: Environmental* **1998**, *16*, 359–374.

43. Yashnik, S. A.; Ismagilov, Z. R.; Anufrienko, V. F. Catalytic Properties and Electronic Structure of Copper Ions in Cu-ZSM-5. *Catalysis Today* **2005**, *110*, 310–322.

44. Groothaert, M. H.; Lievens, K.; Leeman, H.; Weckhuysen, B. M.; Schoonheydt, R. A. An Operando Optical Fiber UV-vis Spectroscopic Study of the Catalytic Decomposition of NO and N2O over Cu-ZSM-5. *Journal of Catalysis* **2003**, *220*, 500–512.

45. Smith, L. J.; Davidson, A.; Cheetham, A. K. A Neutron Diffraction and Infrared Spectroscopy Study of the Acid Form of the Aluminosilicate Zeolite, Chabazite (H-SSZ-13). *Catalysis Letters* **1998**, *49*, 143–146.

46. Fernandez, A.-B.; Marinas, A.; Blasco, T.; Fornes, V.; Corma, A. Insight into the Active Sites for the Beckmann Rearrangement on Porous Solids by in Situ Infrared Spectroscopy. *Journal of Catalysis* **2006**, *243*, 270–277.

47. Heinichen, H. K.; Holderich, W. F. Acylation of 2-Methoxynaphthalene in the Presence of Modified Zeolite HBEA. *Journal of Catalysis* **1999**, *185*, 408–414.

48. Choi, S. Y.; Park, Y. S.; Hong, S. B.; Yoon, K. B. Iodine as a Visible Probe for the Evaluation of Zeolite Donor Strength. *Journal of the American Chemical Society* **1996**, *118*, 9377–9386.

49. Jia, C.; Massiani, P.; Barthomeuf, D. Characterization by Infrared and Nuclear Magnetic Resonance Spectroscopies of Calcined Beta Zeolite. *Journal of the Chemical Society, Faraday Transactions* **1993**, *89*, 3659–3665.

50. Swanson, H. E.; Tatge, E. Standard X-ray Diffraction Powder Patterns. *National Bureau of Standards Circular (U. S.)* **1953**, *539*, 95 pp.

51. McMurdie, H. F.; Morris, M. C.; Evans, E. H.; Paretzkin, B.; Wong-Ng, W.; Ettlinger, L.; Hubbard, C. R. Standard X-ray Diffraction Powder Patterns from the JCPDS Research Associateship. *Powder Diffraction* **1986**, *1*, 64–77.

52. A. C. M., D. B. Van; J., G. Van; R. A., S. Van Preparation of Highly Dispersed Platinum Particles in HZSM-5 Zeolite: a Study of the Pretreatment Process of [Pt(NH3)4]2+. *Journal of Catalysis* **1997**, *167*, 417–424.

53. Tkachenko, O. P.; Klementiev, K. V; Loeffler, E.; Ritzkopf, I.; Schueth, F.; Bandyopadhyay, M.; Grabowski, S.; Gies, H.; Hagen, V.; Muhler, M.; *et al.* The Structure of Zinc and Copper Oxide Species Hosted in Porous Siliceous Matrices. *Physical Chemistry Chemical Physics* **2003**, *5*, 4325–4334.

54. Li, F.; Jiang, Y.; Xia, M.; Sun, M.; Xue, B.; Liu, D.; Zhang, X. Effect of the P/Ti Ratio on the Visible-light Photocatalytic Activity of P-doped TiO2. *Journal of Physical Chemistry C* **2009**, *113*, 18134–18141.

55. Iwase, M.; Yamada, K.; Kurisaki, T.; Prieto-Mahaney, O. O.; Ohtani, B.; Wakita, H. Visible-light Photocatalysis with Phosphorus-doped titanium(IV) Oxide Particles Prepared Using a Phosphide Compound. *Applied Catalysis, B: Environmental* **2013**, *132-133*, 39–44.

56. Benarafa, A.; Kacimi, M.; Coudurier, G.; Ziyad, M. Characterisation of the Active Sites in Butan-2-ol Dehydrogenation over Calcium-copper and Calcium-sodium-copper Phosphates. *Applied Catalysis, A: General* **2000**, *196*, 25–35.

57. Bamberger, C. E.; Specht, E. D.; Anovitz, L. M. Crystalline Copper Phosphates: Synthesis and Thermal Stability. *Journal of the American Ceramic Society* **1997**, *80*, 3133–3138.

58. Roldan, R.; Beale, A. M.; Sanchez-Sanchez, M.; Romero-Salguero, F. J.; Jimenez-Sanchidrian, C.; Gomez, J. P.; Sankar, G. Effect of the Impregnation Order on the Nature of Metal Particles of Bi-functional Pt/Pd-supported Zeolite Beta Materials and on Their Catalytic Activity for the Hydroisomerization of Alkanes. *Journal of Catalysis* **2008**, *254*, 12–26.

59. Song, L.; Zhang, S. Preparation and Visible Light Photocatalytic Activity of Bi2O3/CaO Photocatalysts. *Reaction Kinetics, Mechanisms and Catalysis* **2010**, *99*, 235–241.

60. McEwen, J.-S.; Anggara, T.; Schneider, W. F.; Kispersky, V. F.; Miller, J. T.; Delgass, W. N.; Ribeiro, F. H. Integrated Operando X-ray Absorption and DFT Characterization of Cu-SSZ-13 Exchange Sites During the Selective Catalytic Reduction of NOx with NH3. *Catalysis Today* **2012**, *184*, 129–144.

61. Goblentz Society IR Spectra for Ammonium Nitrate http://webbook.nist.gov/cgi/cbook.cgi?ID=C6484522&Units=SI&Mask=80#IR-Spec (accessed Aug 14, 2013).

62. Hamada, H. Selective Reduction of NO by Hydrocarbons and Oxygenated Hydrocarbons over Metal Oxide Catalysts. *Catalysis Today* **1994**, *22*, 21–40.

B APPENDIX

i The used heating programs

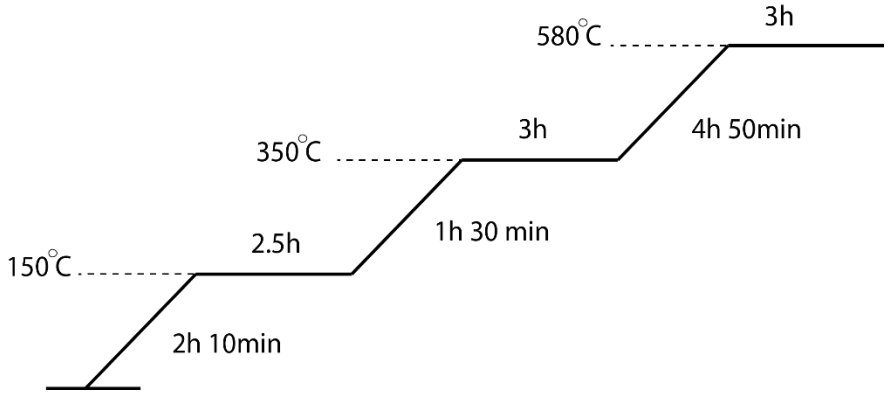

Figure B-1: The temperature ramp used for calcination of the synthesized SSZ-13 to remove the template and to form the H-SSZ-13 zeolite.

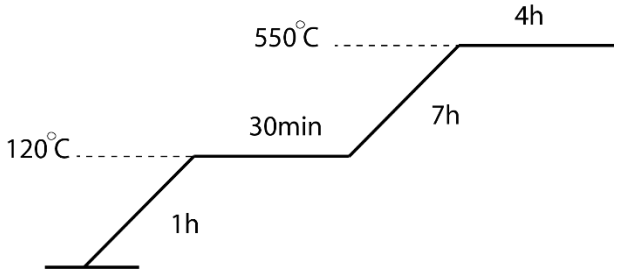

Figure B-2: The temperature ramp used for calcination of the ion-exchanged SSZ-13.

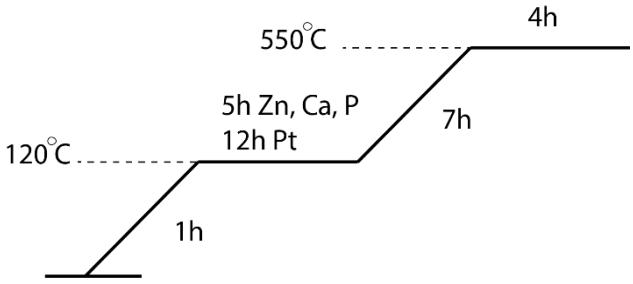

Figure B-3: The temperature ramp used for calcination of the impregnated samples. For Pt, longer 12h dwell at 120 °C used due to higher solution amount used in impregnation.

ii The steaming program

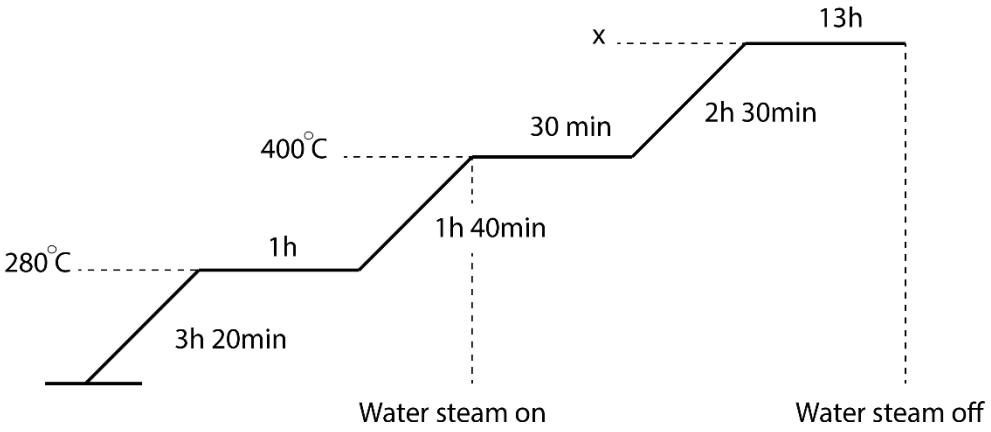

Figure B-4: The temperature program used to steam the Cu-SSZ-13 samples. x = 610 °C, 690°C, 730 °C or 820 °C depending on the sample. Program similar to the one devised by Moliner *et al.,* reproduced from reference 34.

B APPENDIX

iii The used gas flow program

Table B-1: The used real gas flows and the program for the catalytic tests performed.

Phase	Gas flows [ml/min]
Dehydration 150 °C	328 ml/min He; 36 ml/min O_2
SCR 150 °C	303 ml/min He; 18 ml/min O_2; 7 ml/min 5%NH_3/He; 32 ml/min 1%NO/He
Raise to 250 °C	328 ml/min He; 36 ml/min O_2
SCR 250 °C	303 ml/min He; 18 ml/min O_2; 7 ml/min 5%NH_3/He; 32 ml/min 1%NO/He
Raise to 350 °C	328 ml/min He; 36 ml/min O_2
SCR 350 °C	303 ml/min He; 18 ml/min O_2; 7 ml/min 5%NH_3/He; 32 ml/min 1%NO/He
Raise to 450 °C	328 ml/min He; 36 ml/min O_2
SCR 450 °C	303 ml/min He; 18 ml/min O_2; 7 ml/min 5%NH_3/He; 32 ml/min 1%NO/He
Cool down to room temperature	328 ml/min He; 36 ml/min O_2

B APPENDIX

iv Some $DeNO_x$ IR absorption spectra and gas profiles

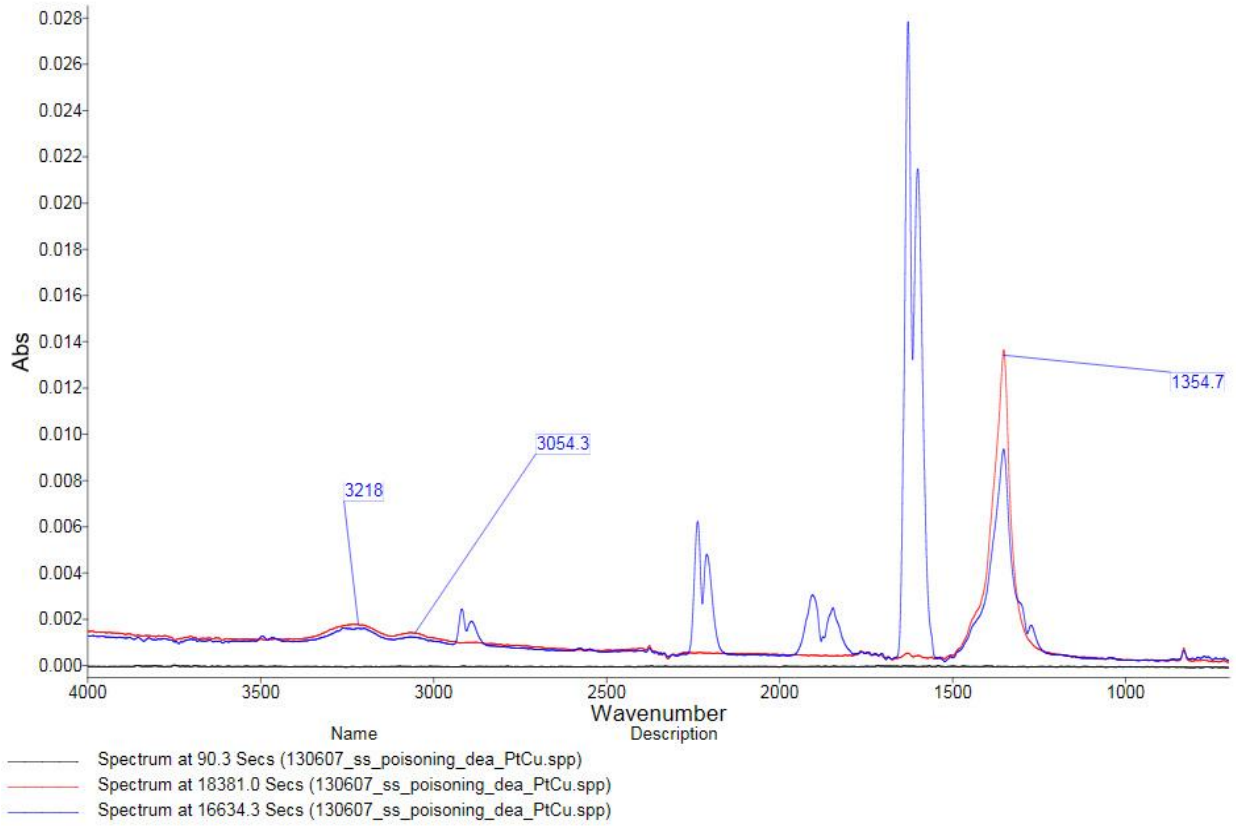

Figure B-5: The gas absorption spectrum from $DeNO_x$ IR from the catalytic test for the Pt impregnated sample. The profile (the red line) here is shown after the reaction at 450 °C while 450 ml/min of He and 50 ml/min of O_2 were flowing through the system. During the course of the catalytic testing, the peaks 3218 cm^{-1}, 3054 cm^{-1} and 1354 cm^{-1} were accumulated (compare the blue and red lines which are taken at different times during the experiment). No decrease in the mentioned peaks was observed even after prolonged time under flow of 450 ml/min of He and 50 ml/min of O_2. The peaks can be assigned to NH_4NO_3, (see reference 61) which seems to have adsorbed on the unheated $DeNO_x$ IR cell.

B APPENDIX

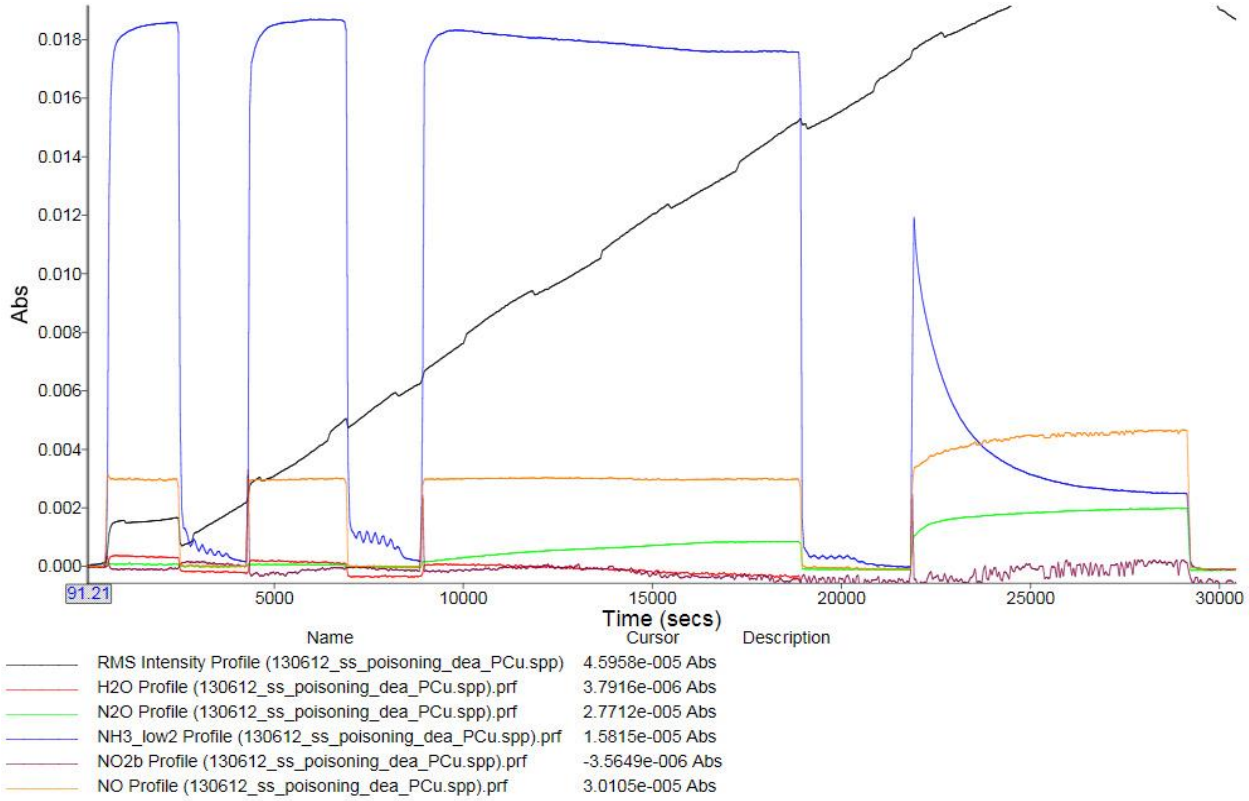

Figure B-6: The gas profile for $DeNO_x$ IR from the catalytic test for the P impregnated sample. The absorption peaks from left to right represent measurements in increasing reaction temperatures; 150 °C, 250 °C, 350 °C and 450 °C, respectively. As can be seen, for temperatures 150-350 °C the NO absorption stays constant i.e. the input NO is just flowing through the system unreacted. At 450 °C, the NO absorption increases i.e. more NO is in the output stream than fed. As can be seen from the NH_3 absorption at 450 °C; it decreases as NO increases, i.e. NH_3 is converted to NO. Also, on both, at temperatures 350 °C and 450 °C some N_2O is formed which is probably sourced to NH_3 as it is the gas consumed as seen from the lowering absorptions.